nature cell biology

ARF1 is directly involved in dynamin-independent endocytosis

Sudha Kumari[1] and Satyajit Mayor[1,2]

Endocytosis of glycosylphosphatidyl inositol (GPI)-anchored proteins (GPI-APs) and the fluid phase takes place primarily through a dynamin- and clathrin-independent, Cdc42-regulated pinocytic mechanism. This mechanism is mediated by primary carriers called clathrin-independent carriers (CLICs), which fuse to form tubular early endocytic compartments called GPI-AP enriched endosomal compartments (GEECs). Here, we show that reduction in activity or levels of ARF1 specifically inhibits GPI-AP and fluid-phase endocytosis without affecting other clathrin-dependent or independent endocytic pathways. ARF1 is activated at distinct sites on the plasma membrane, and by the recruitment of RhoGAP domain-containing protein, ARHGAP10, to the plasma membrane, modulates cell-surface Cdc42 dynamics. This results in the coupling of ARF1 and Cdc42 activity to regulate endocytosis at the plasma membrane. These findings provide a molecular basis for a crosstalk of endocytosis with secretion by the sharing of a key regulator of secretory traffic, ARF1.

Internalization of cargo at the cell surface takes place via multiple clathrin-dependent and independent pathways[1–3]. Many of these mechanisms use the large GTPase dynamin to facilitate vesicle fission at the plasma membrane, although other pathways function in its absence. A dynamin-independent, Cdc42-regulated pinocytic pathway is one such example[4]; it does not use the coat-proteins, caveolin or clathrin, nor the scission effector, dynamin. Nascent endocytic vesicles (CLICs) in this pathway have been recently identified[5], and they fuse to form early endosomal intermediates, GEECs[4]. This is distinct from the early sorting endosomal compartment which also contains clathrin-dependent endocytic cargo[6]. Although the GEEC pathway is responsible for endocytosis of specific components of the membrane such as GPI-APs and cholera toxin (CTx) bound to its ganglioside receptor (GM1), it also facilitates pinocytosis in a variety of cell lines[4–8].

Recently, we have shown that cholesterol-sensitive Cdc42 activation results in recruitment of actin-polymerization machinery to specific foci at the plasma membrane, promoting endocytosis via CLICs into GEECs[9]. This results in an endocytic pathway that is sensitive to perturbations of cholesterol levels and actin polymerization. To date, very few other components of this pathway have been identified. Flotillin1 has been reported to be required for internalization via a clathrin and dynamin independent pathway[10], and CtBP1–BARS protein has been implicated in a dynamin-independent pinocytic mechanism[11]. Further downstream, Rab5 and PI(3)K are recruited to early endocytic intermediates of the GEEC pathway, resulting in fusion with sorting endosomes[6].

The functional significance of endocytosis via GEECs is expanding as we discover both specific cargo and molecular players that participate in this pathway; for example, folate uptake via GPI-anchored folate receptors (FR-GPI), and the internalization of vacuolating toxins such as VacA and aerolysin, are mediated by this pathway[3,12]. Taking into account the diverse functions of GPI-AP cargo and the importance of fluid-phase endocytosis for a variety of cellular processes, it is imperative to understand the molecular mechanism of the GEEC pathway.

Here, we have examined the role of the ADP-ribosylation factor (ARF) family of proteins that participate in multiple intracellular trafficking events[13]. Of the many family members[13], ARF1 and ARF6 are the best characterized. ARF1 has a central role in vesicle formation during early and late secretory traffic[14,15], whereas ARF6 is involved in regulating the actin cytoskeleton near the cell surface and has been implicated in multiple pathways of endocytosis[16–8]. We find that activated ARF1 is present at the plasma membrane and recruits ARHGAP10, a GAP for Cdc42, which, in turn, regulates endocytosis via the GEEC pathway.

RESULTS

Modulation of ARF1 GTPase activity specifically affects endocytosis via the GEEC pathway

ARF1, a cytosolic GTPase with a relative molecular mass of 21,000 (M_r, 21K), is recruited to Golgi membranes, where its location in the membrane depends on GTP-binding[19]. The GDP-exchange deficient form of ARF1 (ARF1^{T31N}) is primarily cytosolic, and behaves as dominant negative isoform of ARF1 activity when overexpressed[20]. To study the effect

[1]National Centre for Biological Science (TIFR), Bellary Road, Bangalore 560 065, India.
[2]Correspondence should be addressed to S.M. (e-mail: mayor@ncbs.res.in)

Received 18 September 2007; accepted 29 November 2007; published online 16 December 2007; DOI: 10.1038/ncb1666

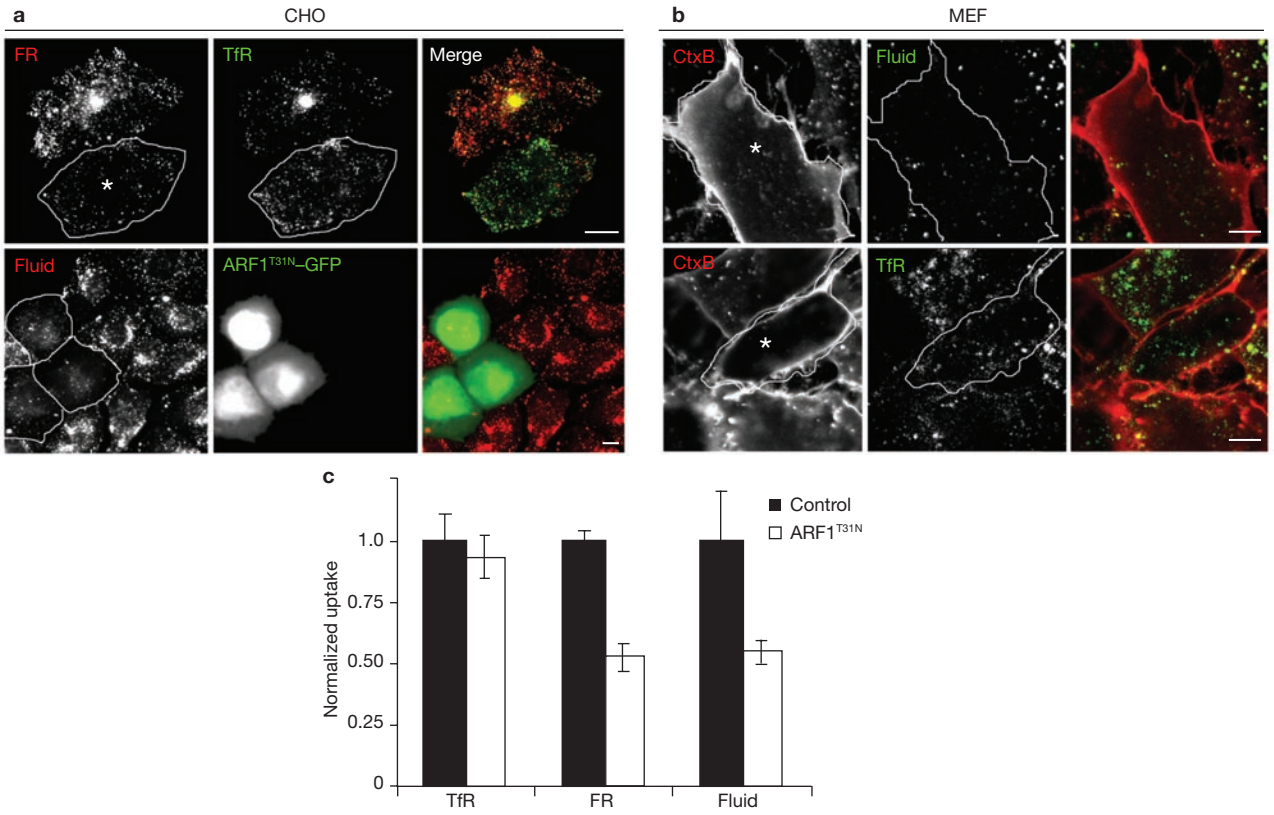

Figure 1 GDP-exchange deficient ARF1 inhibits uptake of GPI-APs and the fluid-phase. (**a**) IA2.2 cells (CHO cells expressing FR-GPI (FR) and human TfR) were transiently transfected with ARF1^{T31N}–GFP (outlined cells) for 18 h, and pulsed with Alexa^{568}Mov19 Fabs and Alexa^{647} Tf (upper panels) or TMR–Dex (lower panels) for 10 min and processed for imaging. Images of internalized FR (red), TfR (green) and the fluid-phase (Fluid; red), are shown in grey-scale and colour merge. In transfected IA2.2 cells, the intracellular distribution of TfR containing perinuclear recycling compartment (REC) is altered, but Tf-uptake is unaffected. (**b**) MEFs transfected with ARF1^{T31N}–GFP for 20 h, were pulsed with labelled probes for 5 min, fixed and imaged on a confocal microscope. Grey-scale and colour merge images of internalized Cy5–CTxB (CTx; red) with TMR–Dex (lower panel; green) or Alexa^{568}Tf (upper panel; green) from a single confocal section are shown (transfected cells are outlined). In transfected cells, uptake of CTxB is blocked and fluid uptake is significantly reduced while TfR-uptake is unaffected. (**c**) Histogram showing uptake of TfR, FR-GPI (normalized to surface receptor expression level) and fluid-phase in ARF1^{T31N} transfected cells plotted as a ratio to corresponding uptake measured in control cells. The error bars represent the weighted mean of fluorescence intensities ± s.e.m. (n = 61, 68, 100, 77, 63, 68; asterisks represent the cells transfected withARF1^{T31N}). The scale bars in **a** and **b** represent 10 μm.

of ARF1 on different pathways of endocytosis, uptake of endocytic cargo specific for each pathway in ARF1^{T31N}-overexpressing CHO cells was quantitatively assessed (Fig. 1a). Endocytosis via the dynamin-dependent pathways, clathrin, caveolin or the RhoA-dependent processes were monitored by measuring the extent of endocytosis of fluorescently-labelled transferrin (Tf) bound to the transferrin receptor (TfR), C_6-Bodipy-lactosylceramide (C_6-LacCer) incorporated into the plasma membrane, or antibodies against the β-subunit of the interleukin 2 receptor (IL2R-β)[21], respectively. Endocytosis via the GEEC pathway was assessed by monitoring uptake of surface-labelled folate receptor (FR–GPI) and TMR-labelled Dextran (TMR–Dex), as probes for GPI-APs and the fluid-phase, respectively. Overexpression of ARF1^{T31N} resulted in specific inhibition of FR–GPI and TMR–Dex uptake, whereas internalization of Tf (Fig. 1a) and C_6-LacCer (see Supplementary information, Fig. S1a) were unaffected. Although ARF1^{T31N} caused a reduction in the surface levels of the IL2R-β, possibly due to its effect on IL2R-β exocytosis, endocytosis of IL2R-β was also unaffected (see Supplementary information, Fig. S1d).

The effect of ARF1^{T31N} on the CLIC–GEEC pathway was not restricted to CHO cells. ARF1^{T31N} expression inhibited FR–GPI and fluid-phase uptake in BHK cells (see Supplementary information, Fig. S2a), and the uptake of GEEC cargo, CTxB and fluid-phase in mouse embryonic fibroblasts (MEFs; Fig. 1b)[5,6]. In cells overexpressing ARF1^{T31N}, steady-state levels of surface FR–GPI were increased (see Supplementary information, Fig. S2c), consistent with inhibition of GPI-AP endocytosis. ARF1 also plays a role in GPI-AP exocytosis, as surface delivery of GPI-APs (see Supplementary information, Fig. S2b) was also inhibited. In parallel, there was a reduction in surface levels of TfR (see Supplementary information, Fig. S2d), and together with alteration in morphology of TfR containing perinuclear-recycling compartment (Fig. 1a), these results suggest a role for ARF1 in the exocytosis of TfR and in TfR recycling[22].

ARF1 depletion inhibits uptake via the GEEC pathway

ARF1^{T31N} overexpression could inhibit endocytosis via GEECs by sequestering GDP exchange factors (GEFs) for other ARF family members, besides ARF1, as some GEFs have overlapping specificity for ARF1 and ARF6 (ref. 23). To discount this possibility, ARF1 protein was depleted using RNA interference (RNAi) methodology[22]. Approximately 60 h post-transfection with *ARF1*-specific short hairpin RNA (shRNA), cells appeared morphologically distinct (see Supplementary information, Fig. S2e) and ARF1 protein levels were reduced (Fig. 2b). The differences

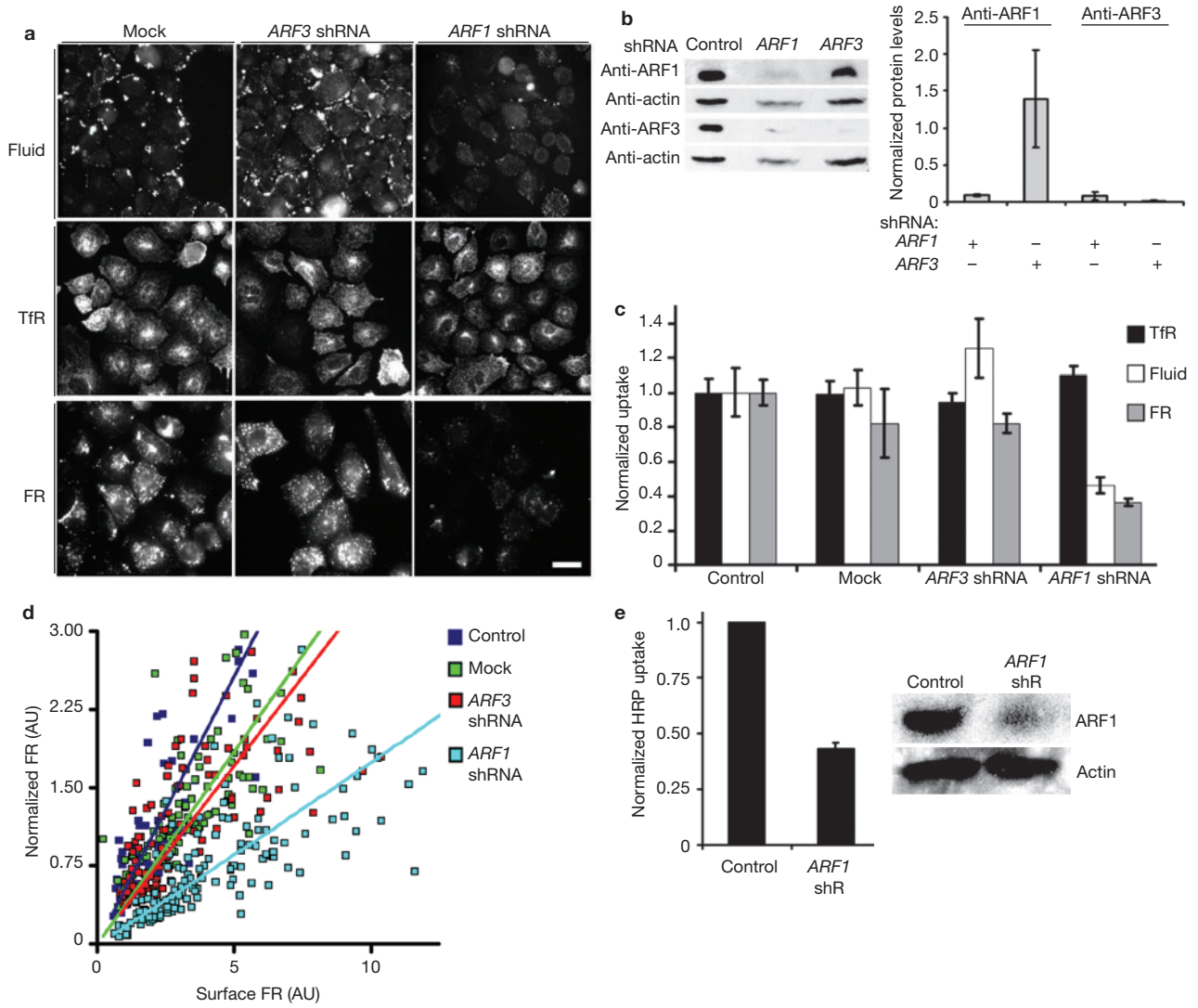

Figure 2 GEEC pathway is inhibited by depletion of ARF1 protein. (**a**, **b**) IA2.2 cells cotransfected with pEGFP-N1 and the indicated shRNA or pSUPER vector (mock) were monitored for endocytosis as described in Fig. 1 (**a**) or harvested for western blotting (**b**). The histogram (**b**) shows the average (± s.d.) of data from three experiments of normalized levels of ARF1 and ARF3 in cells sorted for GFP fluorescence, where the amount of ARF protein as detected on western blots is normalized to the actin level per lane, and expressed as a ratio with respect to the value obtained in mock-transfected sample. (**c**) Histogram showing quantification of endocytosed probes in the cells expressing GFP, where each bar represents endocytosed fluorescence intensity (normalized surface receptor expression, TfR and FR) expressed relative to that measured in mock-transfected cells. Values plotted are weighted mean ± s.e.m. (n = 126, 116, 91, 95, 96, 103, 92, 90, 113, 100, 110). (**d**) Scatter graph (and trend lines) showing variation of endocytosed PLR (FR–GPI) probe fluorescence intensities versus surface FR–GPI levels in individual cells transfected with indicated shRNA, from ≥80 cells per condition. FR–GPI uptake in cells was measured by monitoring endocytosed PLR as above, and surface levels of FR–GPI were quantified by measuring cell surface Cy5–Mov19 binding capacity. (**e**) Histogram showing the amount of endocytosed HRP in cells transfected with vector alone (control) or *ARF1* shRNA. Each bar represents the average of HRP activity normalized to the control, from two representative experiments ± s.d. Western blot shows the extent of reduction in ARF1 levels in cells taken for HRP uptake assays. The scale bar in **a** represents 20 μm.

in actin levels observed between control and shRNA-transfected cells may have resulted from the unequal number of cells loaded in different lysates. Although surface-receptor normalized Tf-uptake was unaffected, FR–GPI and the fluid-phase uptake were markedly reduced (Fig. 2a, c and d). Similar results were observed with another shRNA sequence against *ARF1* (data not shown). A reduction in fluid-phase uptake by ARF1 shRNA-treated cells was also confirmed by a biochemical assay, using horseradish peroxidase (HRP) as a fluid-phase probe (Fig. 2e).

ARF1 depletion decreased both the number of fluid-containing endosomes and average endosomal intensities (see Supplementary information, Fig. S3a, b and c). Furthermore, reduction in FR–GPI uptake after treatment with ARF1 shRNA was not due to decreased cell-surface levels, as FR-GPI endocytosis was reduced in ARF1 depleted cells at comparable surface levels of FR–GPI (Fig. 2d). Similarly to results obtained with $ARF1^{T31N}$ expression, ARF1 depletion caused a reduction in cell-surface levels of TfR, consistent with previous studies on the role of ARF1 in membrane recycling to the plasma membrane[22,24]. In ARF1-depleted cells, there was a detectable reduction in ARF3 levels (Fig. 2b). As the ARF1 target sequences do not share any significant sequence similarity with ARF3, this could be a result of coregulation of the protein products in CHO cells; however, further experiments are required to confirm this possibility. To directly test the involvement of ARF3, cells were transfected with

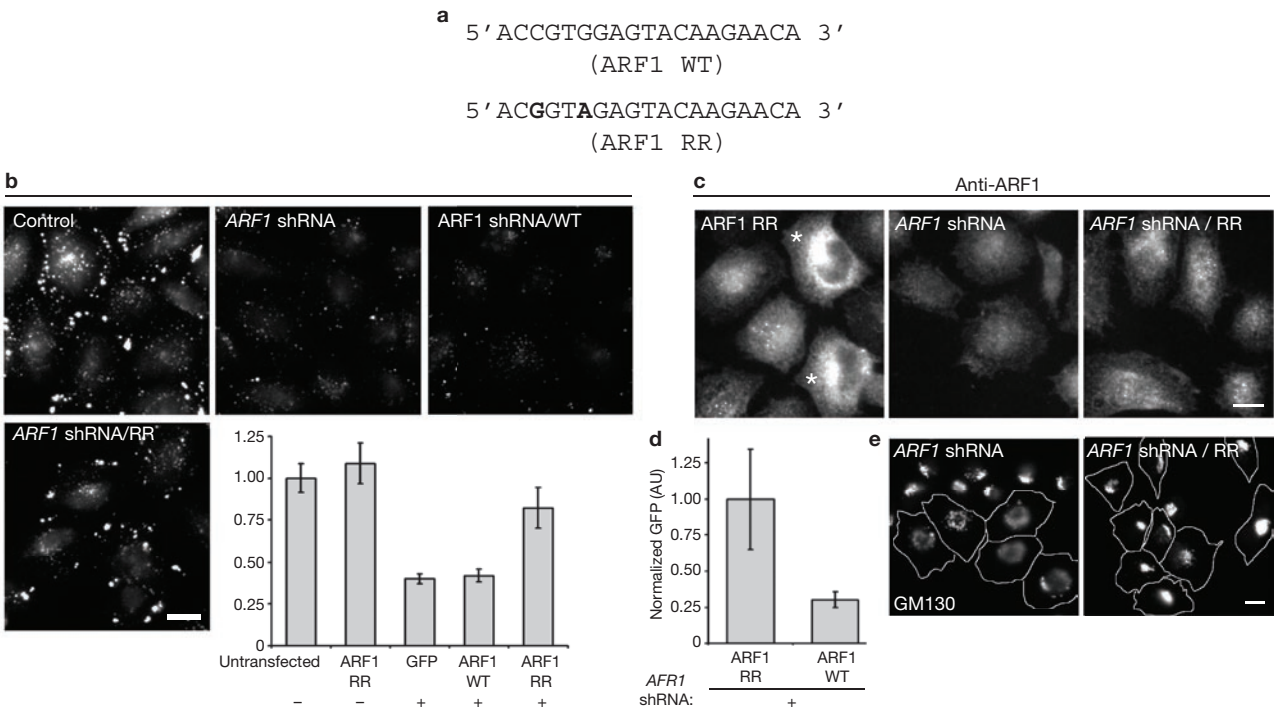

Figure 3 RNAi-resistant ARF1 reverts shRNA-mediated inhibition of the GEEC pathway. (**a**) Silent nucleotide substitutions in primers employed to create *ARF1* RNAi-resistant (RR) form are highlighted in bold-type, with respect to positions in wild-type (WT) ARF1. (**b**) IA2.2 cells transfected with ARF1 RR–GFP (control), *ARF1* shRNA alone, or *ARF1* shRNA and ARF1 WT–GFP (*ARF1* shRNA/WT), or *ARF1* shRNA and ARF1 RR–GFP (*ARF1* shRNA/RR), were assessed for endocytosis of the fluid phase 60 h post-transfection. The histogram shows the quantification of fluid uptake in the indicated GFP-expressing cells. The error bars represent weighted mean, normalized to untransfected (control) cells, ± s.e.m.(n = 89, 81, 109, 84, 97). This experiment was repeated twice with similar results. (**c**) Cells transfected with indicated expression vectors for 60 h were fixed and processed for immunofluorescence microscopy to detect ARF1 levels. ARF1 RR–GFP overexpressing cells are marked with an asterisk. Note that coexpression of ARF1 RR–GFP with shRNA restores the ARF1-antibody staining levels comparable to unmarked cells in ARF1 RR panel. (**d**) Histogram representing the average GFP-fluorescence intensity in cells cotransfected with *ARF1* shRNA together with ARF1 WT–GFP or ARF1 RR—GFP, normalized to GFP fluorescence levels in ARF1 RR–GFP transfected cells. The error bars represent weighted mean of GFP intensities detected in individual cells (arbitrary units, AU) ± s.e.m.(n = 120, 91). This experiment was repeated twice with similar results. (**e**) Overexpression of ARF1 RR–GFP in *ARF1* shRNA transfected cells restores typical Golgi morphology as assessed by monitoring GM130 antibody staining pattern. Approximately 70% of cells transfected with *ARF1* shRNA exhibited a disrupted Golgi pattern. Note GM130 staining in the shRNA-expressing outlined cell versus surrounding untransfected cells. In contrast, only approximately 30% of cells exhibit this phenotype in cells cotransfected with ARF1 RR–GFP (n ≥80). The scale bars in **b**, **c** and **e** represent 10 μm.

shRNA against *ARF3* (Fig. 2a, c) and endocytosis was measured. In ARF3-depleted cells, ARF3 levels were reduced without altering ARF1 levels (Fig. 2b); however, there was no reduction in fluid-phase, TfR or FR–GPI uptake (Fig. 2a, c). Similarly in cells depleted of ARF4 or ARF5, there was no detectable reduction in fluid uptake (see Supplementary information, Fig. S4). Moreover, expression of an RNAi-resistant form of ARF1 (Fig. 3a) that rescues the levels of ARF1 protein (Fig. 3c, d) restored fluid-phase uptake significantly (Fig. 3b). In cells transfected with ARF1 shRNA, Golgi morphology was altered to a more hazy appearance. Consistent with rescue of ARF1 function, the morphology of the Golgi was also restored in cells expressing the RNAi-resistant construct when cotransfected with shRNA against *ARF1* (Fig. 3e). In contrast, depletion of ARF6 by shRNA did not affect endocytosis via the GEEC pathway (see Supplementary information, Fig. S3d). These results provide evidence that ARF1 is specifically required for endocytosis via the GEEC pathway.

Involvement of ARF1 in the GEEC pathway is distinct from its role in secretion

Recently, perturbation of Syntaxin6 function was shown to inhibit caveolar uptake in human foreskin fibroblasts via inhibition of delivery of specific membrane components from the Golgi[25]. One explanation for the inhibition of endocytosis is an indirect effect by inhibition of membrane traffic from the Golgi to the plasma membrane, as perturbation of ARF1 inhibits Golgi-to-cell surface delivery of GPI-APs and other cargo[22,26,27] (see Supplementary information, Fig. S2b). Many secretory mutants in yeast are also known to have endocytic defects[28]. To test this hypothesis, cells were treated with Brefeldin A (BFA), a fungal metabolite that inhibits Golgi-to-cell surface traffic[29] by blocking some ARF-GEFs and causing release of Golgi-localized ARF[30,31]. At concentrations of BFA where Golgi disassembly occurs, cell-surface delivery of newly synthesized GPI-AP (CFP–GPI) was inhibited (Fig. 4a). However, endocytosis of fluid phase and GPI-APs was measurably enhanced (Fig. 4b) via the GEEC pathway; endosomes formed during BFA-treatment contain endocytosed FITC–Dex and FR–GPI, but not Tf (see Supplementary information, Fig. S5a). A similar increase in uptake of a fluid-phase marker, HRP, on BFA treatment, has been reported in apical membrane of MDCK cells[32]. BFA treatment redistributed perinuclear-localized endocytosed Tf into extensive tubular compartments (data not shown) and reduced cell-surface levels of TfR, as previously reported[33], but did not affect the internalization of Tf (Fig. 1a and see Supplementary information, Fig. S5c). Importantly, BFA-mediated increase in uptake via the GEEC pathway was reversed by ARF1^{T31N} expression (Fig. 4c).

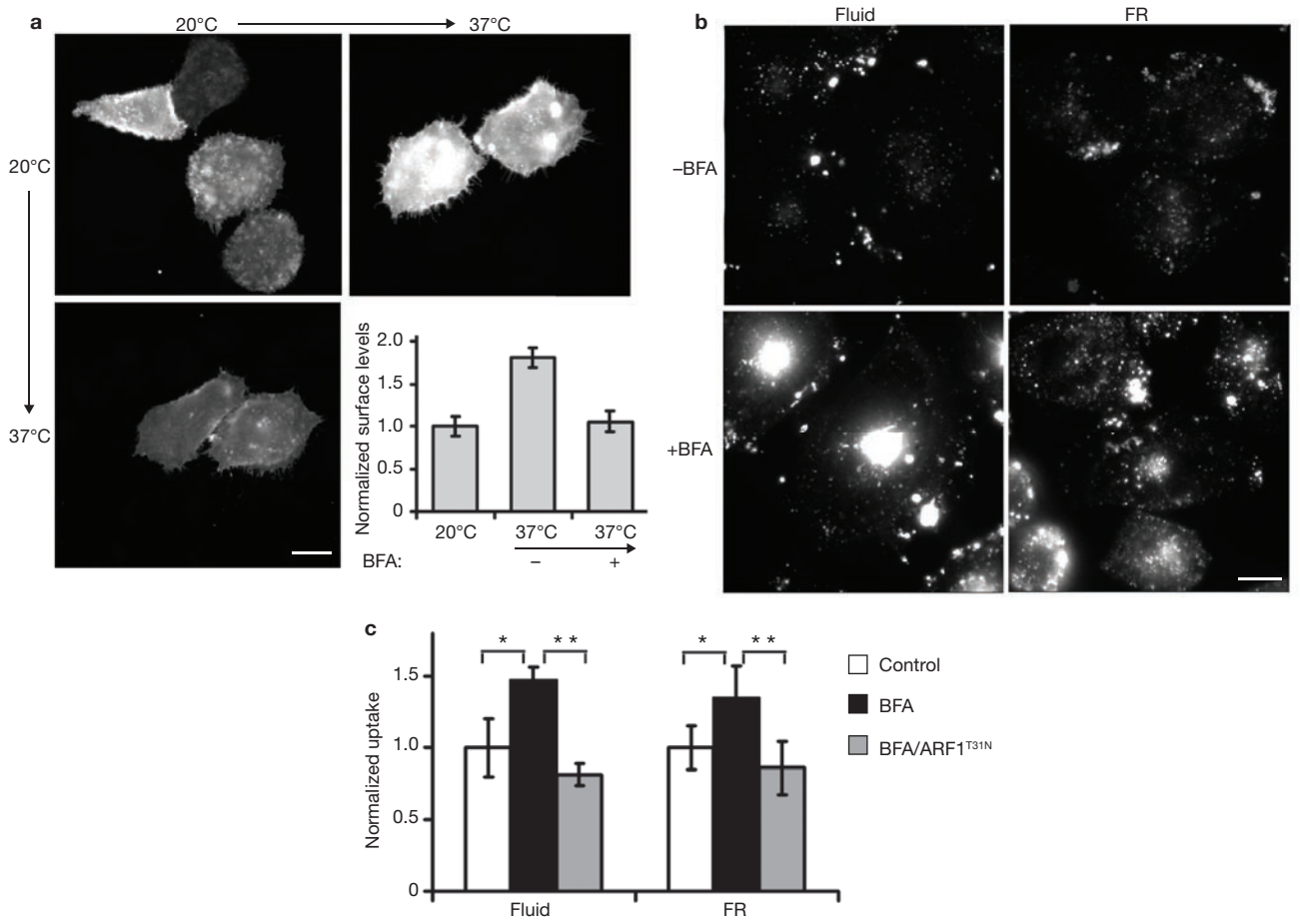

Figure 4 Brefeldin A inhibits surface delivery of GPI-APs, but enhances endocytosis via the GEEC pathway. (**a**) CHO cells transiently transfected with CFP–GPI were grown at 20 °C for 16 h and then shifted to 37 °C in presence (+BFA, 20 μg ml^{-1}) or absence of Brefeldin A (–BFA) for 1 h. Surface levels of CFP–GPI, monitored by labelling cells with anti-CFP at 4 °C, shows that BFA-treatment blocks exocytic delivery of CFP–GPI. The histogram shows anti-CFP antibody fluorescence at the surface of cells, normalized to total CFP–GPI expression per cell, and plotted as a ratio to the cell surface levels measured at 20 °C. The error bars represent weighted mean ± s.e.m. (n = 56, 40, 55). (**b**) IA2.2 cells, treated with BFA (20 μg ml^{-1} for 1 h at 37 °C) were assayed for FR–GPI and the fluid-phase uptake as described in Fig. 1. In BFA-treated cells, fluid-phase and FR–GPI uptake is enhanced. (**c**) Histogram showing quantification of fluorescence of endocytosed probes (normalized to FR–GPI expression at the surface for FR-GPI uptake) in cells treated with BFA in the presence or absence of ARF1^{T31N} transfection, represented as the ratio of uptake to that observed in untreated cells (control). The error bars represents weighted mean ± s.e.m. (n = 98, 139, 71 for fluid and 103, 112, 64 for FR). The single and double asterisks represent P values (<0.002) from the indicated comparisons. The scale bars in **a** and **b** represent 10 μm.

Thus, ARF1 is directly required for endocytosis via GEEC pathway, and not indirectly via modulation of exocytic delivery of specific membrane components. These results also demonstrate that ARF1 function in the GEEC pathway is BFA-insensitive, implicating a BFA-resistant GEF in ARF1 activation at the plasma membrane.

ARF1 modulates GEEC pathway via the adaptor ARHGAP10

ARF1 recruits ARHGAP10, a multi-domain protein (M_r 200K) identified in yeast–two hybrid interaction screen of constitutively active ARF1 and ARF6 (refs 34, 35). ARHGAP10 has a distinct domain (ABD) necessary for binding activated ARF1, and a GAP domain for RhoGTPases (R-G; Fig.5a). ABD encompasses a plekstrin homology (PH) domain, which does not bind to PtdIns, but is essential for ARF binding; the R-G domain possesses a relatively high GAP activity for Cdc42 compared with other Rho GTPases, and mutation of Arg 1183 to alanine in the R-G domain renders it incapable of GAP activity[34]. When overexpressed, these domains function as dominant-negative inhibitors for the generation of actin- patches on the Golgi[34]. To determine whether ARHGAP10 could couple the activation of ARF1 with a GAP activity for Cdc42, and in turn affect GPI-AP endocytosis, different domains of this protein were expressed (Fig. 5b). All the truncated domains, with the exception of the mutated RhoGAP domain, were capable of marginal but significant inhibition of endocytosis via GEECs (Fig. 5b), but not Tf uptake (see Supplementary Information, Fig. S5c).

Overexpression of ARF1^{Q71L}, an isoform of ARF1 deficient in GTP hydrolysis, lead to increased FR–GPI internalization, as well as a more peripheral distribution of FR–GPI endosomes (Fig. 5b, c), suggesting a role for ARF1 in post-endocytic trafficking. Persistent activation of ARF1 was also accompanied by a reduction in Tf uptake (see Supplementary information, Fig. S5c). This could arise due to sequestration of shared GTPase activating proteins (GAPs) for ARF1 and ARF6 that are reported to be involved in clathrin-mediated endocytosis[17]. To determine whether ARHGAP10 exerts its effect downstream of activated ARF1, we examined whether coexpression of ARHGAP10

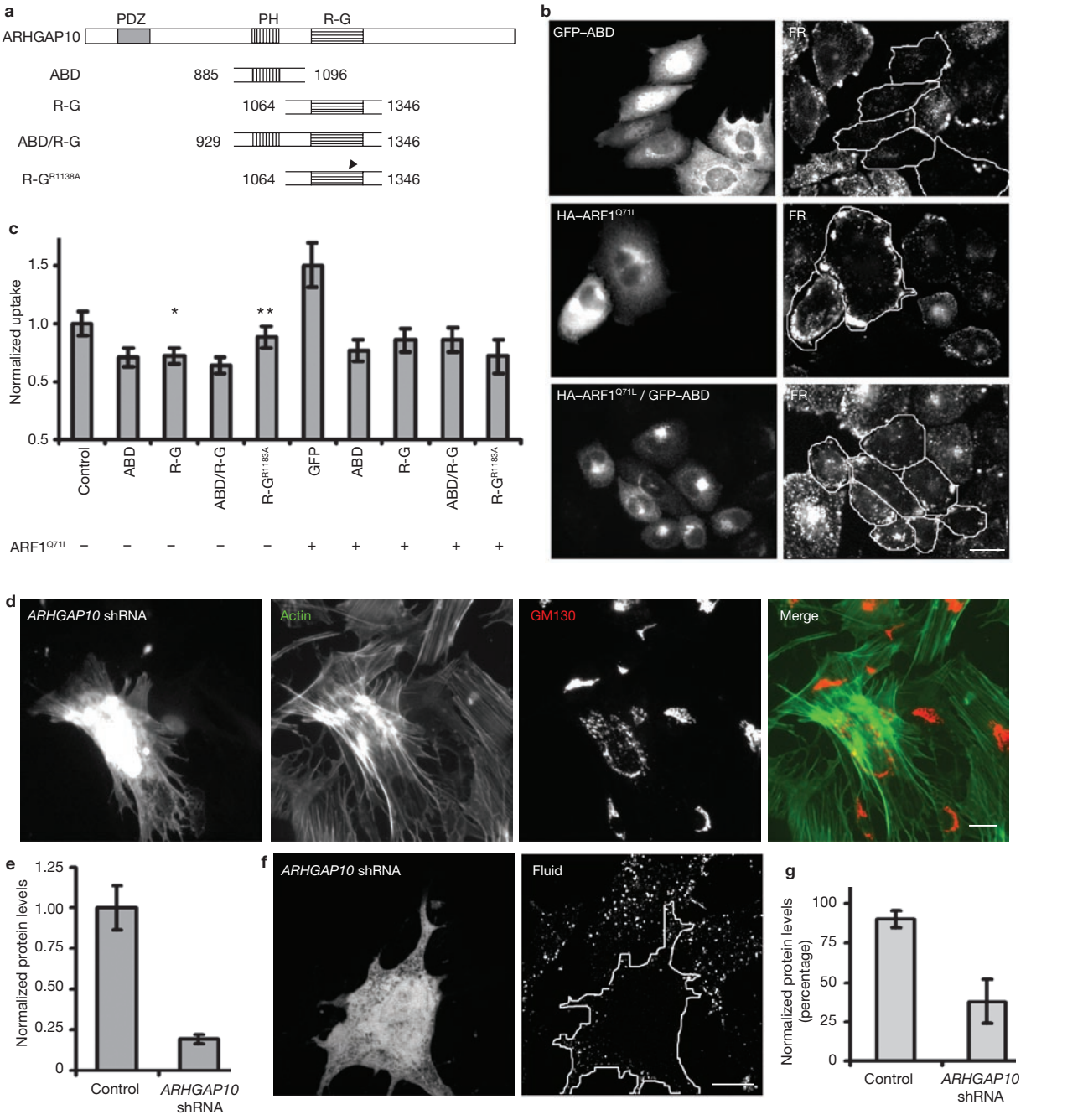

Figure 5 ARF1 functions via ARHGAP10. (**a**) Deletion constructs of ARHGAP10 with different domains. ARF binding domain, ABD; RhoGAP domain, R-G; ABD and R-G domain, ABD/R-G; R-G domain mutated for GAP activity, R-G^{R1183A}. (**b**) IA2.2 cells transfected with either singly with GFP–ABD, HA–ARF1^{Q71L} or with both constructs were assayed for endocytosis of FR–GPI. Expression of GFP–ABD reduces, whereas ARF1^{Q71L} expression enhances FR–GPI uptake. Endocytosed FR–GPI is more peripherally distributed in ARF1^{Q71L}-expressing cells. Coexpression of both proteins (outlined cells) shows that GFP–ABD expression antagonizes ARF1^{Q71L}-mediated endocytic enhancement. (**c**) Histogram showing quantification of internalized FR–GPI in cells expressing the indicated combination of constructs, normalized to that measured in GFP-transfected cells. The error bars represent weighted mean ± s.e.m. (n = 66, 49, 54, 57, 50, 50, 44, 56, 49). The single asterisk and the double asterisk represent P values ≤0.01, and 0.2, respectively. (**d**) MEFs transfected with *ARHGAP10* shRNA for 72 h were fixed and stained for actin organization and Golgi morphology (GM130). Note that in transfected cells, the actin distribution is altered and Golgi is dispersed. This F-actin reorganization is observed in approximately 30% of transfected cells and change in Golgi morphology is observed in approximately 60% cells. (**e**) Histogram showing levels of anti-V5 antibody staining in V5-tagged ARHGAP10 N-terminal domain coexpressed with eGFP-N1 (control) or *ARHGAP10* shRNA in CHO cells. The error bars represent weighted mean of average of V5 intensities per cell ± s.e.m. (n = 97, 82). (**f**) MEFs expressing *ARHGAP10* shRNA (outlined, green in merge) exhibit a reduction in fluid-phase uptake (outlined, right panel) compared with surrounding untransfected cells. Images are single confocal plane representing either transfection marker or internalized fluid. (**g**) Histogram showing the percentage of cells (MEFs) that exhibit a normal fluid-phase uptake in cells expressing GFP alone (control) or *ARHGAP10* shRNA, when compared to untransfected cells. The error bars represent average of data from three independent experiments ± s.d. (n = 35, 56). The scale bars represent 20 μm.

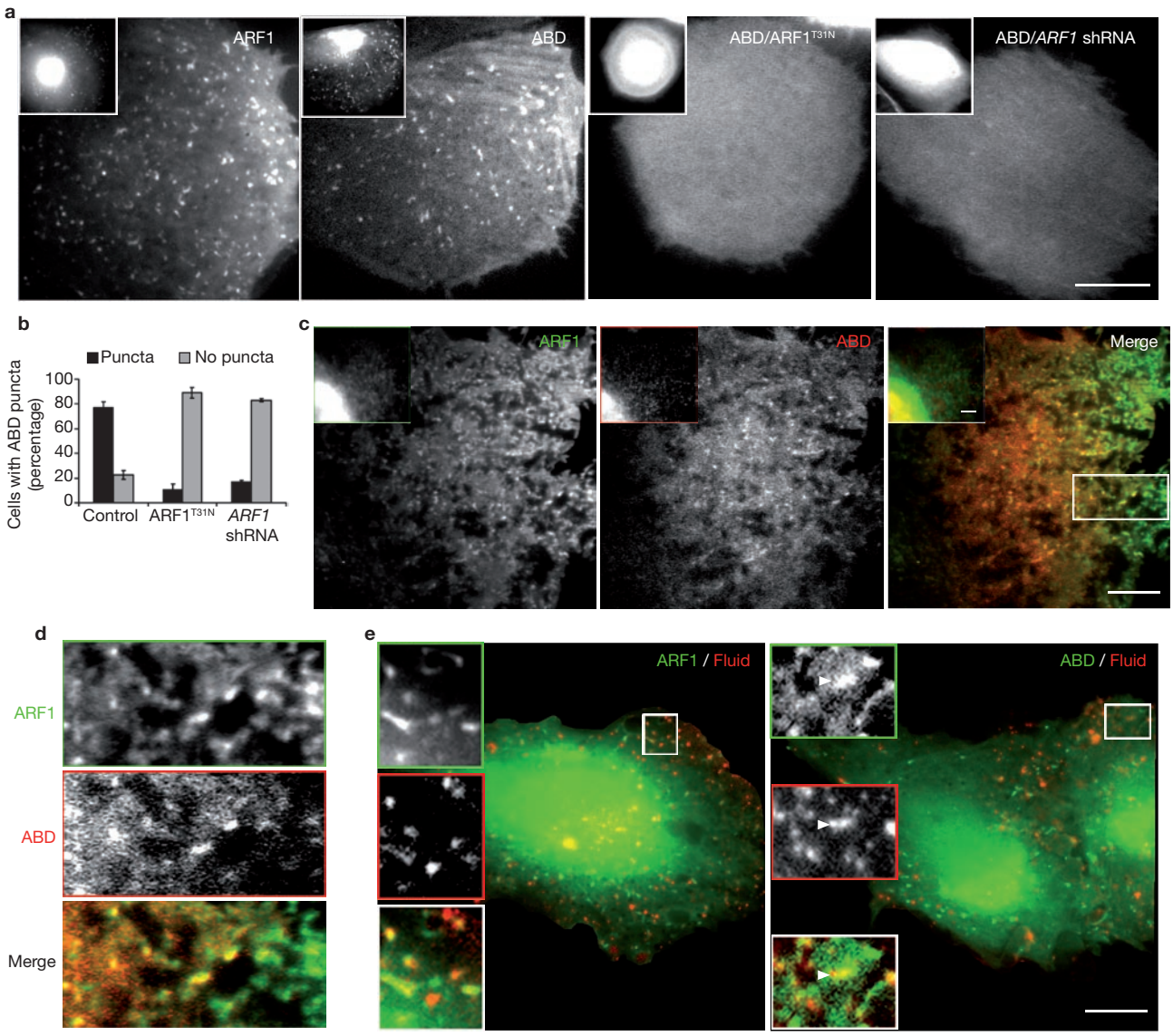

Figure 6 Activated ARF1 is located at the plasma membrane and on fluid-containing nascent endosomes. (**a**) IA2.2 cells transfected with ARF1–GFP and GFP–ABD expression vectors as indicated were sequentially imaged using TIRF and wide-field illumination. ARF1–GFP and GFP–ABD appear enriched on the Golgi in the wide-field (inset), whereas in the same cells distinct punctate foci of these proteins are visible in the TIRF field. Cotransfection of cells with HA–ARF1^{T31N} and *ARF1* shRNA removes these foci from the plasma membrane. (**b**) Histogram showing the fraction of GFP–ABD transfected cells with punctate distribution on cotransfection with ARF1^{T31N} or *ARF1* shRNA. The error bars represent weighted mean ± s.e.m. (n = 45, 36, 42). (**c**) IA2.2 cells transfected with ARF1–GFP and RFP–ABD were imaged live using sequential TIRF illumination. The delay between acquisition of ARF1 and ABD images is 200 ms. Note that in merge of ARF1 and ABD images, all the ABD puncta colocalize with ARF1. A portion of merge (box) is magnified in **e**. (**e**) IA2.2 cells transfected with ARF1–GFP (left, green) or GFP–ABD (right, green) were pulsed with TMR–Dex (Fluid, red) for 40 s at 37 °C, washed, fixed and imaged. Insets show a magnified view of the region demarcated with a square, where there is extensive colocalization of the two colours. The scale bars in **a**, **d** and **e** represent 10 μm.

domains would inhibit enhanced FR–GPI internalization induced by ARF1^{Q71L} (Fig. 5b, c). Different domains of ARHGAP10 reversed the ARF1^{Q71L}-induced enhanced FR–GPI uptake to a similar extent (Fig. 5c). The extent of inhibition of uptake was comparable in R-G- and R-G^{R1183A}-domain expressing cells, suggesting that the interaction between ARHGAP10 and Cdc42 was not dependent on the activity of the GAP domain. Taken together with the inhibition observed in the ABD/R-G domain, these data suggest that full-length ARHGAP10 is required as a link between ARF1 and Cdc42.

The inhibition mediated by the ARHGAP10 domains may be explained by sequestration of activated ARF1 and thus inhibition of ARF1, rather than a dominant-negative of ARHGAP10. To determine a role for ARHGAP10 more specifically, endogenous ARHGAP10 was depleted using shRNA. As hamster *ARHGAP10* sequence is unknown, the effects of shRNA were monitored in MEFs, where the uptake of fluid is ARF1 sensitive (Fig. 1b) and the *ARHGAP10* sequence has been determined. The efficacy of shRNA was confirmed by monitoring the depletion of protein levels of an ARHGAP10 fragment when coexpressed with

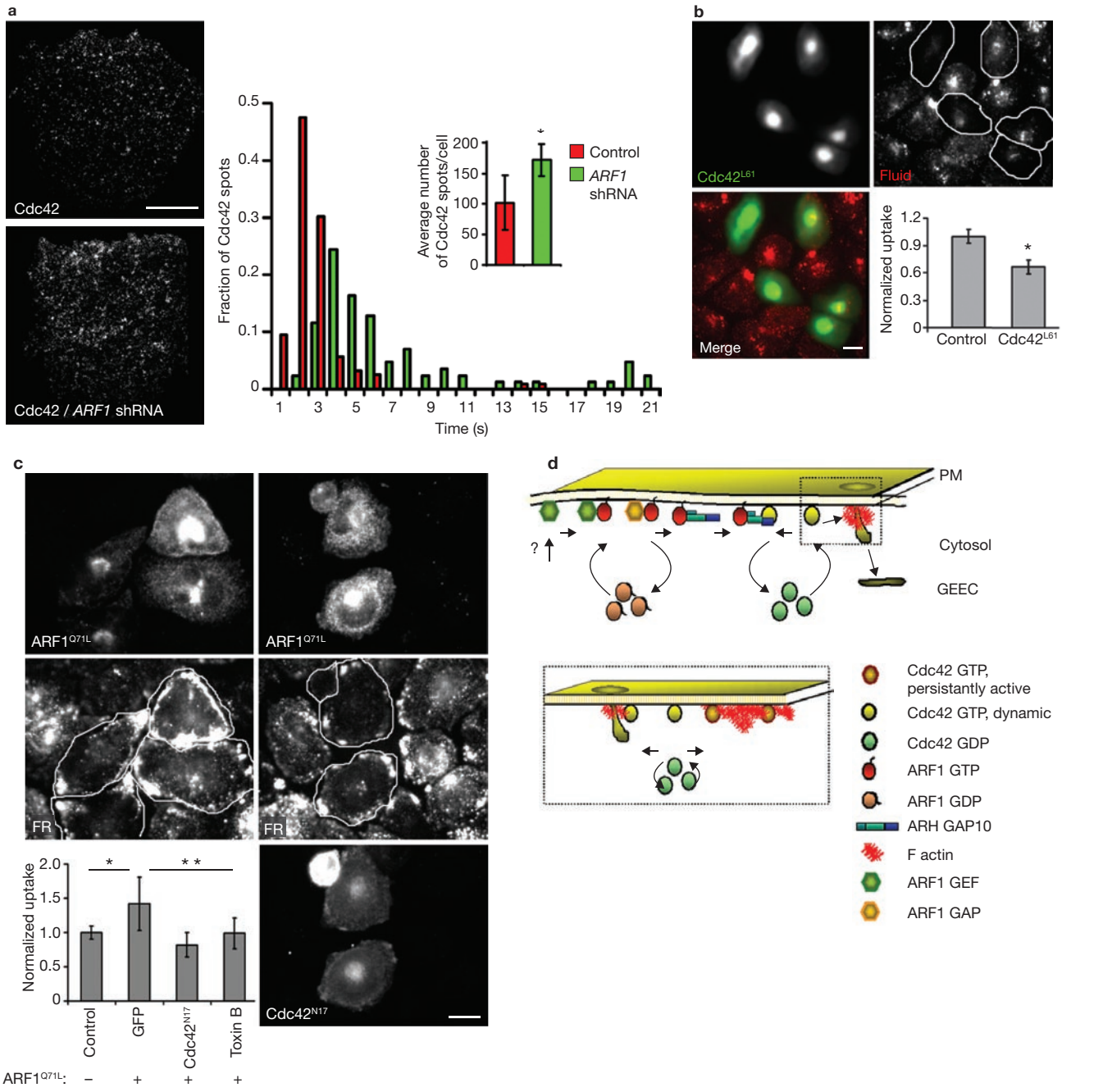

Figure 7 ARF1 activation couples to Cdc42 dynamics at plasma membrane. (**a**) IA2.2 cells expressing Cdc42–GFP, without or with cotransfection of *ARF1* shRNA were imaged at 37 °C under TIRF illumination to visualize distribution of single molecules of Cdc42 at the plasma membrane. The histogram shows that the mean residence time of Cdc42 (indicated by arrows) and the average number of molecules (± s.d.) shown in the inset, increase in *ARF1* shRNA transfected cells. Data are from one experiment out of two with similar results, where 12 cells in each condition were analysed. The asterisk indicates $P \leq 0.006$. (**b**) IA2.2 cells transfected with GFP–Cdc42^{L61} (green in merge) were pulsed with TMR–Dex (red in merge), fixed and imaged. The histogram shows the uptake of TMR–Dex in cells expressing GFP–Cdc42^{L61} normalized to untransfected cells from a single experiment, repeated twice with similar results. The error bars represent weighted mean ± s.e.m. ($n = 50, 58$). The asterisk represents $P \leq 0.002$. (**c**) IA2.2 cells transfected with HA–ARF1^{Q71L} either alone or with Cdc42^{N17} were assayed for FR–GPI uptake (FR), and processed for detection of HA–ARF1^{Q71L} and GFP. The histogram shows quantification of endocytosed Alexa568–Mov19 Fab fluorescence (normalized to surface FR–GPI levels) in cells expressing ARF1^{Q71L}, cotransfected with GFP–Cdc42N17, or treated with Toxin B (1 μg ml–1 for 60 min), plotted as a ratio to uptake measured in untransfected (control) cells. The error bars represent weighted mean ± s.e.m. ($n = 60, 78, 73, 79$). The single and double asterisks represent P ≤0.003 for the indicated comparisons. (d) In a model for ARF1-dependent regulation of endocytosis via GEEC pathway, ARF1 is activity is governed by a BFA-resistant GEF and a GAP of unknown identity (?). Activated ARF1 recruits ARHGAP10 to function as a RhoGAP for Cdc42, resulting in inactivation and release of Cdc42 into cytosol. Activated Cdc42 regulates dynamic actin polymerization that leads to formation of endosomes via the GEEC pathway. However, persistent activation of Cdc42 (due to constitutively activated Cdc42 or loss of ARHGAP10-based RhoGAP activity) leads to a different type of actin architecture (see box), incompatible with endocytosis via the GEEC pathway. The scale bars in **a**, **b** and **c** represent 10 μm.

shRNA (Fig. 5e), or by monitoring the effects on actin organization and Golgi morphology as described previously[34] (Fig. 5d). In approximately 60% of GFP-expressing cells, the shRNA resulted in alteration in Golgi morphology; fewer cells showed a perturbation of actin organization (approximately 30%). Consistent with this result, expression of shRNA against *ARHGAP10* resulted in approximately 60% of the transfected cells exhibiting a detectable reduction in fluid uptake (Fig. 5f, g). These results implicate ARHGAP10 in uptake via the GEEC pathway, downstream of ARF1 activation, potentially coupling it with GAP activity for Cdc42.

Recruitment of ABD to the plasma membrane is sensitive to ARF1 activation

The involvement of ARF1 in endocytosis at the plasma membrane requires plasma membrane-localized activated ARF1. To observe the distribution of ARF1 at the plasma membrane, total internal reflection fluorescence microscopy (TIRFM) was used to report on distribution of fluorophores in the evanescent field in close proximity (~100 nm for 488nm illumination) to the plasma membane. TIRFM imaging of live cells expressing low levels of ARF1–GFP revealed relatively stable, punctate structures located at the plasma membrane (Fig. 6a and see Supplementary Information, Movie 1) that were resistant to treatment with BFA (see Supplementary Information, Fig. S5b).

To determine whether the recruitment of the ABD at the plasma membrane depends on ARF1 activation, live cells expressing very low levels of GFP-tagged constructs of different ARHGAP10 domains were imaged using TIRFM (Fig. 6a and see Supplementary Information, Fig. S6a). Low levels of expression provided better contrast of detection in TIRFM and did not affect fluid uptake, therefore acting as non-perturbing reporters. Full-length ARHGAP10 was not detectably expressed in cells[34], but similarly to ARF1–GFP, GFP–ABD appeared as relatively stable, punctate structures at the plasma membrane (Fig. 6a). Although GFP–ABD structures were fewer in number than ARF1–GFP, they mimicked both the morphology and distribution of ARF1 puncta. Similar punctuate patterns were observed for ABD/R-G, which can bind to activated ARF1 and Cdc42, but the R-G domain (lacking ABD) was uniformly distributed (see Supplementary information, Fig. S6a). To determine whether ABD is a sensor of ARF1 activation, it was coexpressed with ARF1 shRNA or HA-tagged ARF1^{T31N} (Fig. 6a). In both cases, GFP–ABD was not recruited to the plasma membrane and appeared similar to cytosolic GFP[9]. Furthermore, RFP–ABD punctae colocalized with ARF1–GFP in the TIRFM field (Fig. 6c, d), but not with ARF6–GFP (see Supplementary Information, Fig. S6b–d).

These observations provide evidence for endogenous ARF1 activation and localization at or near the plasma membrane, and support the use of ABD as a reporter for endogenous ARF1 activation. The recruitment of ABD to activated ARF1 sites in the plasma membrane is consistent with the coupling of activated ARF1 to ARHGAP10 in the plasma membrane.

Activated ARF1 is located on early intermediates of the GEEC pathway

If ARF1 activity is required for endocytosis via the GEEC pathway, colocalization of activated ARF1 on nascent endocytic carriers of the GEEC pathway should be observed. For this purpose, cells were pulsed with TMR–Dex for short times (60 s) and imaged. A fraction of fluid-containing endosomes colocalized with GFP–ABD-labelled vesicles and tubules (Fig. 6e) and colocalization was also observed with ARF1–GFP (Fig. 6e). Newly formed fluid and FR–GPI containing endocytic carriers did not colocalize with coat components such as COPI (known to interact with ARF1 on Golgi and some endosomal membranes[31]), even in the presence of ARF1^{Q71L} (see Supplementary information, Fig. S5d).

ARF1 influences Cdc42 dynamics on plasma membrane

To address the role of ARF1 in regulating Cdc42 dynamics at the plasma membrane, the recruitment of Cdc42 to the plasma membraned was monitored using live-cell TIRFM, both in control cells and after silencing endogenous ARF1 (Fig. 7a). The extent of recruitment, and plasma membrane residence time, of single molecules of Cdc42 are positively influenced by GTP-bound status of Cdc42 (ref. 9). Depletion of ARF1 enhanced both the number of Cdc42 recruitment events and its residence time (Fig. 7a and see Supplementary Information, Movie 2), and formation of cortical spike-like structures (see Supplementary Information, Fig. S2e), consistent with activation of Cdc42 at the plasma membrane[9,36,37]. Furthermore, similarly to ARF1 silencing, overexpression of a constitutively active form of Cdc42 (Cdc42^{L61}) led to reduction in fluid-phase uptake (Fig. 7b).

To determine whether the coupling of ARF1 activation and Cdc42 dynamics can influence endocytosis via the GEEC pathway, GPI-AP endocytosis was monitored in cells overexpressing ARF1^{Q71L}. Coexpression of Cdc42^{N17} (a GTP-exchange deficient form[4]) or treatment with Toxin B (an inhibitor of Rho GTPases) reverted the activated ARF1^{Q71L}-mediated increase in GEEC endocytosis (Fig. 7c). These results provide evidence that ARF1 is part of the molecular machinery that regulates the GEEC pathway, upstream of Cdc42.

DISCUSSION

ARF1 has been extensively studied in COPI-coated vesicle formation at the Golgi[38], and it is also involved in recruiting AP3 and COPI subunits to endosomal membrane buds in PC12 cells[31,39]. A recent report using a heterologously expressed sensor for activated ARFs detected BFA-insensitive sequential activation of ARF6 followed by ARF1 at sites of phagocytosis[40].

Our data, using a variety of techniques including RNAi depletion, dominant-negative inhibition and dominant-active activation, support a model (Fig. 7d) wherein activated ARF1 is directly and specifically involved in endocytosis via the Cdc42-regulated GEEC pathway at the cell surface.

There are several lines of evidence that support a role for ARHGAP10 as the downstream effector of activated ARF1 at the plasma membrane, providing the critical GAP-activity necessary for Cdc42 cycling: first, activated ARF1 directly binds to ARHGAP10 (ref. 34) and silencing ARHGAP10 inhibits endocytosis via the GEEC pathway; second, ARF1-binding fragments of ARHGAP10 (ABD) block ARF1^{Q71L}-induced activation of the GEEC pathway, as well as the constitutive operation of this pathway; and third, ABD exhibits a dynamic punctate distribution at the plasma membrane colocalized with ARF1, and maintained by activated ARF1, as depletion of ARF1 or overexpression of ARF1^{T31N} prevents recruitment of the ABD domain. Although ABD serves as a specific reporter for ARF1 on the plasma membrane, ABD is also capable of interacting with both ARF6 and ARF1 on intracellular structures — although much higher expression levels of ARF6 are required for visualizing the colocalization of ABD–RFP and ARF6 (see Supplementary Information, Fig. S6). This difference may arise due to differences in membrane composition at plasma membrane and endomembranes, such that association with ARF1 is more favoured at some regions on the plasma membrane.

These regions could mark the sites where endocytosis via GEECs is initiated by enhancing the local cycling kinetics of Cdc42.

The coupling of ARF1 activation with a Cdc42–GAP activity is supported by the observation that depletion of ARF1 or ARF1^{T31N} expression (data not shown) results in persistently activated Cdc42 at the plasma membrane, as assessed by single-molecule TIRFM. As expression of both GTP-binding and GTPase-deficient mutants of Cdc42 inhibit endocytosis via GEECs, these results support a role for ARF1-activation in dynamic cycling of Cdc42, required for endocytosis via GEECs. Activated Cdc42 is recruited to the plasma membrane and initiates actin polymerization, thereby promoting endocytosis via GEECs in an actin-dependent mechanism[9]. This is reminiscent of ARF1–ARHGAP10 in actin-patch formation at the Golgi[34]. Likewise, it is possible that the ARF–ARHGAP10 interaction can also aid other endomembrane transport processes, the involvement of these molecular interactions in intracellular trafficking processes is not clear as yet.

The involvement of ARF1 in endocytosis demands a source of activated ARF1 and its effectors (GAPs and GEFs) at the plasma membrane. Our data show that the GEF involved in ARF1 activation is BFA insensitive. Similar observations have been reported in studies on the uptake of FM4-64 in maize root-hair cells[41] and phagocytosis in macrophages[40], where endocytosis is blocked on overexpression of ARF1^{T31N}, but not by BFA treatment. A recent report has shown that a BFA resistant ARF–GEF, GNL1 is required for selective internalization at the plasma membrane in *Arabidopsis* root-hair cells[42]. The BFA-insensitive GEF could be a member of ARNO–Cytohesin family[43]. However, expression of deletion mutants of ARNO failed to inhibit GPI-AP's uptake (S.K., unpublished observations), suggesting the use of other GEF(s). Another regulator of dynamin-independent endocytic pathways is the CtBP1–BARS protein, which is reported to aid vesicle fission[11]. It is interesting that the ARF1-specific GAP protein, ARFGAP1, interacts directly with BARS, and is hypothesized to function as a dynamin counterpart[44]. ARFGAP1 may provide a link for interaction of ARF1 based machinery with CtBP1–BARS.

These studies suggest that endocytosis via the GEEC pathway could be limited by the availability of activated ARF1 at the plasma membrane in a wide variety of cell lines, including a human cell line (S.K., unpublished observations), and support a central role for ARF1 where it is necessary for endocytosis via GEECs, but do not exclude an ancillary role for ARF3 — ARFs have been reported to function in combination in specific trafficking processes[22].

Activated ARF1 (detected by ABD-GFP staining) is also found on nascent endocytic structures that contain the fluid phase and have the characteristic tubular morphology of CLICs and GEECs[5]. However, at this time, we cannot determine whether ARF1 is derived directly from the cell surface or independently recruited to CLICs–GEECs, post-internalization. Thus, in addition to its role at the plasma membrane, ARF1 may have other roles in the GEEC pathway. Endocytic carriers stimulated by expression of ARF1^{Q71L} do not colocalize with COPI (β-COP) in fixed cells; ARF1 may recruit other endosomal coats onto GEECs, such as AP3 on endosomes in PC12 cells[39] or other molecules[15]. Overexpression of ARF1^{Q71L} leads to peripheral distribution of FR endosomes, suggesting a role in post-endocytic trafficking as well.

ARF6 is also thought to regulate a clathrin and dynamin-independent endocytic pathway[3,16]. As ARF6 depletion or inhibition[6] has no effect on uptake into GEECs, this argues that the ARF6- and Cdc42-regulated pathways are either distinct processes operating differentially in different cell types, or that ARF6 could modify the ARF1–Cdc42-regulated pathway, post-internalization in some cell types.

In conclusion, we find that multiple proteins, which have a Golgi-enriched steady-state distribution, are involved in regulating endocytosis via the dynamin-independent pinocytic (GEEC) pathway. In addition to ARF1, CtBP1–BARS and Cdc42 are both enriched in the Golgi[11,45]. The involvement of yet another central secretory traffic regulator, ARF1 in endocytosis, raises an interesting possibility that exocytosis and endocytosis may be integrated for maintenance of plasma membrane homeostasis[2]. In addition, our data suggest that this is likely to be accomplished by regulated spatial distribution of distinct ARF1 effectors, and will be a focus of future studies.

METHODS

Cell culture, reagents, and plasmids. See Supplementary Information, Methods.

Synthesis of RNAi-resistant ARF1 and shRNA against *ARF6* and *ARHGAP10*. RNAi-resistant ARF1 was generated by using a primer 5′-ATAGGCTTCAACG TGGAAAC**G**GT**A**GAGTACAAGAACATCAGCTTC-3′, where the nucleotide sequences corresponding to the *ARF1* RNAi sequence used were altered as indicated in bold type. This primer was used to amplify human ARF1–GFP using PCR. The resultant plasmid was sequenced verified before use. *ARF6* shRNA (sequence corresponding to 307–327 nucleotides of human ARF6 coding sequence; 5′-CCAGGAGCTGCACCGCATTAT-3′), was chosen as target sequence. This sequence is conserved in human, mouse and rat *ARF6*. The shRNA against this sequence was ligated into pGSUPER vector, as previously described[46]. A similar procedure was used for generation of *ARHGAP10* shRNA. The sequence chosen was conserved between human and mouse *ARHGAP10* and corresponds to 817–836 in human coding sequence (5′-GTCATTGTGCCTTCTGAGA-3′). For generation of mRFP–ABD, mRFP was obtained from plasmid mRFPpSETb using the primer 5′-ATAGGTACCACCGGTCGCCACCATGGCCTCCTCCGAG-3′. Following the RFP sequence, a 14 bp linker sequence was added such that mRFP sequence is flanked by *Age*I and *Bgl*II enzyme sites. EGFP from pEGFPC2–ABD was replaced with mRFP, using these enzyme sites. All of the above mentioned constructs were used after confirmation of sequence following cloning.

Endocytic and exocytic assays and immunofluorescence microscopy. Endocytic and exocytic assays cells were carried out as previously described[4] with minor modifications, as detailed in the Supplementary Information, Methods.

shRNA transfection and western blotting. shRNA in the pSUPER vector (*ARF1*) was transfected with a fixed ratio of vector carrying the shRNA sequence of interest or pSUPER vector alone (mock) with pEGFP-N1 (3:1, w/w) in 3 cm cover-slip dishes, to ensure cotransfection. Coexpression using this protocol was confirmed by measuring the reduction of protein target levels in GFP-expressing cells by using specific antibodies against the protein target. In all of the endocytic experiments, shRNA was cotransfected with pEGFP-N1 for identification of transfected cells, unless otherwise mentioned. Cells transfected with shRNA directed against *ARF6* in pG-SUPER vectors were identified by GFP coexpression. To biochemically measure protein depletion, cells were plated in 92 mm dishes and cotransfected with shRNA carrying vector or vector alone (control) with pEGFP-N1. Post-transfection, cells were allowed to grow for 60 h, harvested using trypsin–EDTA, and GFP-positive cells were sorted using FACS-Vantage SE (BD, San Jose, CA). Approximately 30,000 sorted cells from each transfection were lysed and loaded on a 12% SDS–PAGE. Protein estimation was carried out after transfer of proteins on PVDF membranes and the regions corresponding to bands of interest on the membrane were cut and probed using anti-ARF1, anti-ARF6, anti-ARF3 or anti-actin antibodies. The band intensities were subsequently quantified.

Imaging, image processing and quantification. Confocal microscopy was carried out on a Zeiss LSM 510 Meta imaging system (63× 1.4 NA; Zeiss, Jena, Germany) or Andor Spinning Disc confocal imaging system (60× 1.42 NA or 100× 1.4 NA, with

Ixon EMCCD; Andor Technologies, Belfast, Ireland) using appropriate factory-set filters and dichroics for different fluorophores. Care was taken to avoid fluorophore saturation during acquisition. For quantitative imaging on spinning disc confocal microscope, laser powers and camera gains were maintained constant throughout the experiment. Images acquired using LSM (Zeiss) software or Revolution (Andor) software was converted into TIFF and analysed using Metamorph software. For live imaging, Nikon TE 2000 inverted system equipped with 100× oil objective (NA 1.45) and a cooled CCD cascade camera (Photometrics Inc, Tuscon, AZ) was used. For dual-colour live imaging, cell growth medium was changed to M1 with 0.1% BSA and glucose, and the dishes containing cells were brought to temperature-controlled stage maintained at 37 °C. Images were collected using Metamorph acquisition software.

For quantification of uptake of endocytic tracers, images were obtained using 20×, 0.75 NA objective on widefield microscope (Nikon TE300). The cells from different fields from each dish were defined as regions, and the integrated intensities inside the 'regions' were obtained using the 'region measurement' application of Metamorph. Average and s.d. of integrated intensities per cell from each dish was determined and plotted as weighted mean of these values, as described in statistical analysis section, unless otherwise stated. The number and intensity of endosomes formed in cells pulsed with TMR–Dex (1 mg ml^{-1}) for 3 min at 37 °C were determined by imaging cells at 20 °C. Images were processed and the endosomes were identified, and total number of endosomes and associated intensity were calculated, as previously described[4,6]. Briefly, the images were processed for background correction using Metamorph and threshold using Multispot software, such that all the endosomes with intensity above the background were identified. The number of endosomes, area and integrated intensity per endosome were determined per cell using Multispot.

TIRF imaging was carried out exactly as previously described[9]. Cdc42 spots were defined as pixels with intensity values above autofluorescence and correspond to single molecules of Cdc42–GFP according to criterion previously established criterion[9]. Note, bleaching of single GFP fluorophores occurs over a much longer period than measured for the Cdc42–GFP fluorophores. Only spots that make an appearance within the imaging duration (100 ms per frame, 200 frames stream acquisition) were considered for quantification. The residence time of each spot was manually estimated by determining the number of frames it was visible. The data were binned and expressed as percentage of total number of dynamic spots tracked.

In all cases, images were analysed using Metamorph software and processed for presentation using Adobe Photoshop. Images are displayed at the same contrast-settings for control and treated cells in all display items. The scale bar corresponds to 10 μm, unless otherwise specified.

Statistical analysis. The values plotted are weighted mean, μ_x, obtained from at least two different dishes in each experiment, calculated using the following formula

$$\mu_x = \frac{\sum \frac{n_i \times \bar{X}_i}{\sigma^2_{X_i}}}{\sum \frac{n_i}{\sigma^2_{X_i}}} \qquad \text{Equation 1}$$

where i is the number of cover-slip dishes used in an experiment, X_i is the mean of fluorescence intensities determined for cells in a single dish, n_i the number of cells observed per dish, and σ_{Xi} the s.d. in the measurement. The s.e.m. was determined by the following equation,

$$\text{s.e.m} = \left(\sum \frac{\sigma^2_{X_i}}{n_i}\right)^{1/2} \qquad \text{Equation 2}$$

unless otherwise specified. Minimum number of cells (n) quantified from an individual dish is indicated in the figure legends. Statistical significance was measured using unpaired, two-tail distribution, Student's it-test. Unless specifically mentioned, the P values were <0.001 in all cases reported. Each experiment was repeated three or more times with similar results, unless otherwise stated.

Note: Supplementary Information is available on the Nature Cell Biology website.

ACKNOWLEDGMENTS

We thank M. Kalia and B. Srinag for help with biochemistry, H. Krishnamurthy and Wellcome Trust-aided imaging and flow-cytometry facility at NCBS for help with confocal imaging and sorting transfected cells. We are indebted to: G. D. Gupta for making ARF6 shRNA; R. Alexander for *ARF1* RNAi resistant and mRFP–ABD vectors; N, Sabu for ARHGAP10 shRNA; J. Gruenberg for GFP-tagged wild-type ARF1 and ARF1^{T31N} plasmids; S.G. Ferguson for HA-tagged wild-type ARF1, ARF1^{T31N} and ARF1^{Q71L} constructs; P. Chavrier for GFP–ARHGAP10 domains; R. A. Kahn for ARF1, ARF3, ARF4 and ARF5 shRNA plasmids; R. Vishwakarma for fluorescent folate analogues; S. Bourgoin for ARF6-specific antibodies; and R. E. for C_6-LacCer. We thank other members of the Mayor Laboratory and NCBS for generous support and encouragement. S.K. is supported by a pre-doctoral fellowship from Council of Scientific and Industrial Research (Government of India). Work in S.M.'s laboratory is supported by intramural funds from NCBS, and a J. C. Bose fellowship.

AUTHOR CONTRIBUTIONS

S.K. executed and analysed all experiments. S.K. and S.M. planned all experiments and wrote the manuscript.

Published online at http://www.nature.com/naturecellbiology/Reprints and permissions information is available online at http://npg.nature.com/reprintsandpermissions

1. Conner, S. D. & Schmid, S. L. Regulated portals of entry into the cell. *Nature* **422**, 37–44 (2003).
2. Kirkham, M. & Parton, R. G. Clathrin-independent endocytosis: new insights into caveolae and non-caveolar lipid raft carriers. *Biochim. Biophys. Acta* **1746**, 350–363 (2005).
3. Mayor, S. & Pagano, R. E. Pathways of clathrin-independent endocytosis. *Nature Rev. Mol. Cell Biol.* **8**, 603–612 (2007).
4. Sabharanjak, S., Sharma, P., Parton, R. G. & Mayor, S. GPI-anchored proteins are delivered to recycling endosomes via a distinct cdc42-regulated, clathrin-independent pinocytic pathway. *Dev. Cell* **2**, 411–423 (2002).
5. Kirkham, M. *et al.* Ultrastructural identification of uncoated caveolin-independent early endocytic vehicles. *J. Cell Biol.* **168**, 465–476 (2005).
6. Kalia, M. *et al.* Arf6-independent GPI-anchored protein-enriched early endosomal compartments fuse with sorting endosomes via a Rab5/phosphatidylinositol-3′-kinase-dependent machinery. *Mol. Biol. Cell* **17**, 3689–3704 (2006).
7. Guha, A., Sriram, V., Krishnan, K. S. & Mayor, S. Shibire mutations reveal distinct dynamin-independent and -dependent endocytic pathways in primary cultures of *Drosophila* hemocytes. *J. Cell Sci.* **116**, 3373–3386 (2003).
8. Gauthier, N. C. *et al. Helicobacter pylori* VacA cytotoxin: a probe for a clathrin-independent and Cdc42-dependent pinocytic pathway routed to late endosomes. *Mol. Biol. Cell* **16**, 4852–4866 (2005).
9. Chadda, R. *et al.* Cholesterol-sensitive Cdc42 activation regulates actin polymerization for endocytosis via the GEEC pathway. *Traffic* **8**, 702–717 (2007).
10. Glebov, O. O., Bright, N. A. & Nichols, B. J. Flotillin-1 defines a clathrin-independent endocytic pathway in mammalian cells. *Nature Cell Biol.* **8**, 46–54 (2006).
11. Bonazzi, M. *et al.* CtBP3/BARS drives membrane fission in dynamin-independent transport pathways. *Nature Cell Biol.* **7**, 570–580 (2005).
12. Sabharanjak, S. & Mayor, S. Folate receptor endocytosis and trafficking. *Adv. Drug Deliv. Rev.* **56**, 1099–1109 (2004).
13. D'Souza-Schorey, C. & Chavrier, P. ARF proteins: roles in membrane traffic and beyond. *Nature Rev. Mol. Cell Biol.* **7**, 347–358 (2006).
14. Zhang, C. J. *et al.* Expression of a dominant allele of human ARF1 inhibits membrane traffic *in vivo*. *J. Cell Biol.* **124**, 289–300 (1994).
15. Nie, Z., Hirsch, D. S. & Randazzo, P. A. Arf and its many interactors. *Curr. Opin. Cell Biol.* **15**, 396–404 (2003).
16. Naslavsky, N., Weigert, R. & Donaldson, J. G. Convergence of non-clathrin- and clathrin-derived endosomes involves Arf6 inactivation and changes in phosphoinositides. *Mol. Biol. Cell* **14**, 417–431 (2003).
17. Tanabe, K. *et al.* A novel GTPase-activating protein for ARF6 directly interacts with clathrin and regulates clathrin-dependent endocytosis. *Mol. Biol. Cell* **16**, 1617–1628 (2005).
18. Paleotti, O. *et al.* The small G-protein Arf6GTP recruits the AP-2 adaptor complex to membranes. *J. Biol. Chem.* **280**, 21661–21666 (2005).
19. Vasudevan, C. *et al.* The distribution and translocation of the G protein ADP-ribosylation factor 1 in live cells is determined by its GTPase activity. *J. Cell Sci.* **111,** 1277–1285 (1998).
20. Dascher, C. & Balch, W. E. Dominant inhibitory mutants of ARF1 block endoplasmic reticulum to Golgi transport and trigger disassembly of the Golgi apparatus. *J. Biol. Chem.* **269**, 1437–1448 (1994).
21. Lamaze, C. *et al.* Interleukin 2 receptors and detergent-resistant membrane domains define a clathrin-independent endocytic pathway. *Mol. Cell* **7**, 661–671 (2001).
22. Volpicelli-Daley, L. A., Li, Y., Zhang, C. J. & Kahn, R. A. Isoform-selective effects of the depletion of ADP-ribosylation factors 1-5 on membrane traffic. *Mol. Biol. Cell* **16**, 4495–4508 (2005).
23. Macia, E., Chabre, M. & Franco, M. Specificities for the small G proteins ARF1 and ARF6 of the guanine nucleotide exchange factors ARNO and EFA6. *J. Biol. Chem.* **276**, 24925–24930 (2001).
24. Shen, X. *et al.* Association of brefeldin A-inhibited guanine nucleotide-exchange protein 2 (BIG2) with recycling endosomes during transferrin uptake. *Proc. Natl. Acad Sci. USA* **103**, 2635–2640 (2006).
25. Choudhury, A., Marks, D. L., Proctor, K. M., Gould, G. W. & Pagano, R. E. Regulation of caveolar endocytosis by syntaxin 6-dependent delivery of membrane components to the cell surface. *Nature Cell Biol.* **8**, 317–328 (2006).

26. Ellis, M. A., Miedel, M. T., Guerriero, C. J. & Weisz, O. A. ADP-ribosylation factor 1-independent protein sorting and export from the trans-Golgi network. *J. Biol. Chem.* **279**, 52735–52743 (2004).
27. Yahara, N., Ueda, T., Sato, K. & Nakano, A. Multiple roles of Arf1 GTPase in the yeast exocytic and endocytic pathways. *Mol. Biol. Cell* **12**, 221–238 (2001).
28. Riezman, H. Endocytosis in yeast: several of the yeast secretory mutants are defective in endocytosis. *Cell* **40**, 1001–1009 (1985).
29. Doms, R. W., Russ, G. & Yewdell, J. W. Brefeldin A redistributes resident and itinerant Golgi proteins to the endoplasmic reticulum. *J. Cell Biol.* **109**, 61–72 (1989).
30. Donaldson, J. G., Finazzi, D. & Klausner, R. D. Brefeldin A inhibits Golgi membrane-catalysed exchange of guanine nucleotide onto ARF protein. *Nature* **360**, 350–352 (1992).
31. Gu, F. & Gruenberg, J. ARF1 regulates pH-dependent COP functions in the early endocytic pathway. *J. Biol. Chem.* **275**, 8154–8160 (2000).
32. Prydz, K., Hansen, S. H., Sandvig, K. & van Deurs, B. Effects of brefeldin A on endocytosis, transcytosis and transport to the Golgi complex in polarized MDCK cells. *J. Cell Biol.* **119**, 259–272 (1992).
33. Shin, H. W., Morinaga, N., Noda, M. & Nakayama, K. BIG2, a guanine nucleotide exchange factor for ADP-ribosylation factors: its localization to recycling endosomes and implication in the endosome integrity. *Mol. Biol. Cell* **15**, 5283–5294 (2004).
34. Dubois, T. *et al.* Golgi-localized GAP for Cdc42 functions downstream of ARF1 to control Arp2/3 complex and F-actin dynamics. *Nature Cell Biol.* **7**, 353–364 (2005).
35. Sousa, S. *et al.* ARHGAP10 is necessary for alpha-catenin recruitment at adherens junctions and for *Listeria* invasion. *Nature Cell Biol.* **7**, 954–960 (2005).
36. Hall, A. Rho GTPases and the actin cytoskeleton. *Science* **279**, 509–514 (1998).
37. Yang, L., Wang, L. & Zheng, Y. Gene targeting of Cdc42 and Cdc42GAP affirms the critical involvement of Cdc42 in filopodia induction, directed migration, and proliferation in primary mouse embryonic fibroblasts. *Mol. Biol. Cell* **17,** 4675– 4685 (2006).
38. Spang, A. ARF1 regulatory factors and COPI vesicle formation. *Curr. Opin. Cell Biol.* **14**, 423–427 (2002).
39. Faundez, V., Horng, J. T. & Kelly, R. B. A function for the AP3 coat complex in synaptic vesicle formation from endosomes. *Cell* **93**, 423–432 (1998).
40. Beemiller, P., Hoppe, A. D. & Swanson, J. A. A phosphatidylinositol-3-kinase-dependent signal transition regulates ARF1 and ARF6 during Fcγ receptor-mediated phagocytosis. *PLoS Biol* **4**, e162 (2006).
41. Xu, J. & Scheres, B. Dissection of Arabidopsis ADP-RIBOSYLATION FACTOR 1 function in epidermal cell polarity. *Plant Cell* **17**, 525–536 (2005).
42. Teh, O.K. & Moore, I. An Arf–GEF acting at the Golgi and in selective endocytosis in polarized plant cells. *Nature* **448**, 493–496 (2007).
43. Chardin, P. *et al.* A human exchange factor for Arf contains Sec7- and pleckstrin homology domains. *Nature* **384,** 481–484 (1996).
43. Yang, J. S. *et al.* Key components of the fission machinery are interchangeable. *Nature Cell Biol.* **8**, 1376–1382 (2006).
44. Erickson, J. W., Zhang, C., Kahn, R. A., Evans, T. & Cerione, R. A. Mammalian Cdc42 is a brefeldin A-sensitive component of the Golgi apparatus. *J. Biol. Chem.* **271**, 26850–26854 (1996).
45. Kojima, S., Vignjevic, D. & Borisy, G. G. Improved silencing vector co-expressing GFP and small hairpin RNA. *Biotechniques* **36**, 74–79 (2004).

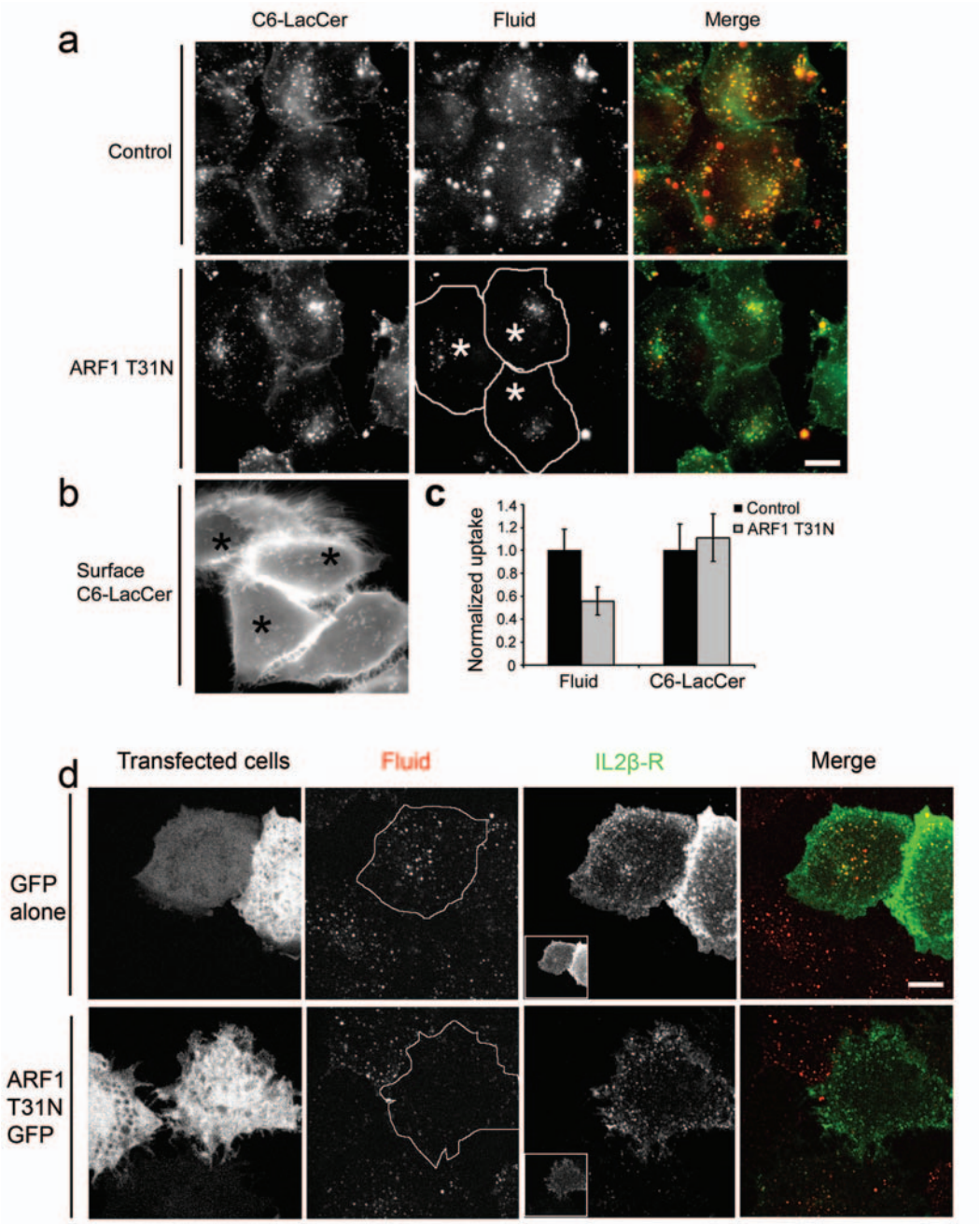

Figure S1 Dominant negative mutants of ARF1 do not affect clathrin-independent but dynamin-dependent endocytic uptake. (a-c) *ARF1-T31N expression does not affect caveolar uptake.* **(a)** IA2.2 cells transfected with RFP alone (control) or along with HA-tagged ARF1-T31N for 18h were pulsed with Alexa^{647}-Dex and C_6-LacCer, washed and processed for imaging. Note uptake of C_6-LacCer is unaffected in cells expressing ARF1-T31N, whereas, Alexa^{647}-Dex internalization is inhibited. **(b)** IA2.2 cells, transfected with ARF1-T31N as above were labeled with C_6-LacCer, excess label was washed off, and the cells were immediately taken for imaging. Note surface labeling of C_6-LacCer is unaffected by ARF1-T31N overexpression, marked with asterisk (*). **(c)** Histogram shows the quantification of the extent of fluid-phase uptake and C_6-LacCer, normalized to control, RFP-transfected cells. This experiment was repeated twice with similar results. Bars are weighted mean +/- SEM. n≥ 25. **d)** *Uptake of IL2R-β is not affected by inhibition of ARF1 activity:* IA2.2 cells cotransfected with IL2R-β and either ARF1-T31N-GFP (left panels) or eGFP-N1 (right panels: control) were labeled with Alexa^{568} anti-IL2R-β on ice for 1h, washed and chased in presence of Alexa^{647}-Dex (fluid) at 37°C for 3min, washed and fixed. The images show the single confocal section in middle plane of the cells. The insets in IL2R-β image show the lowermost section depicting the surface levels of IL2-β in corresponding cells. Note that in cells transfected with ARF1-T31N, while fluid uptake is reduced, anti-IL2R-β uptake is unaffected.

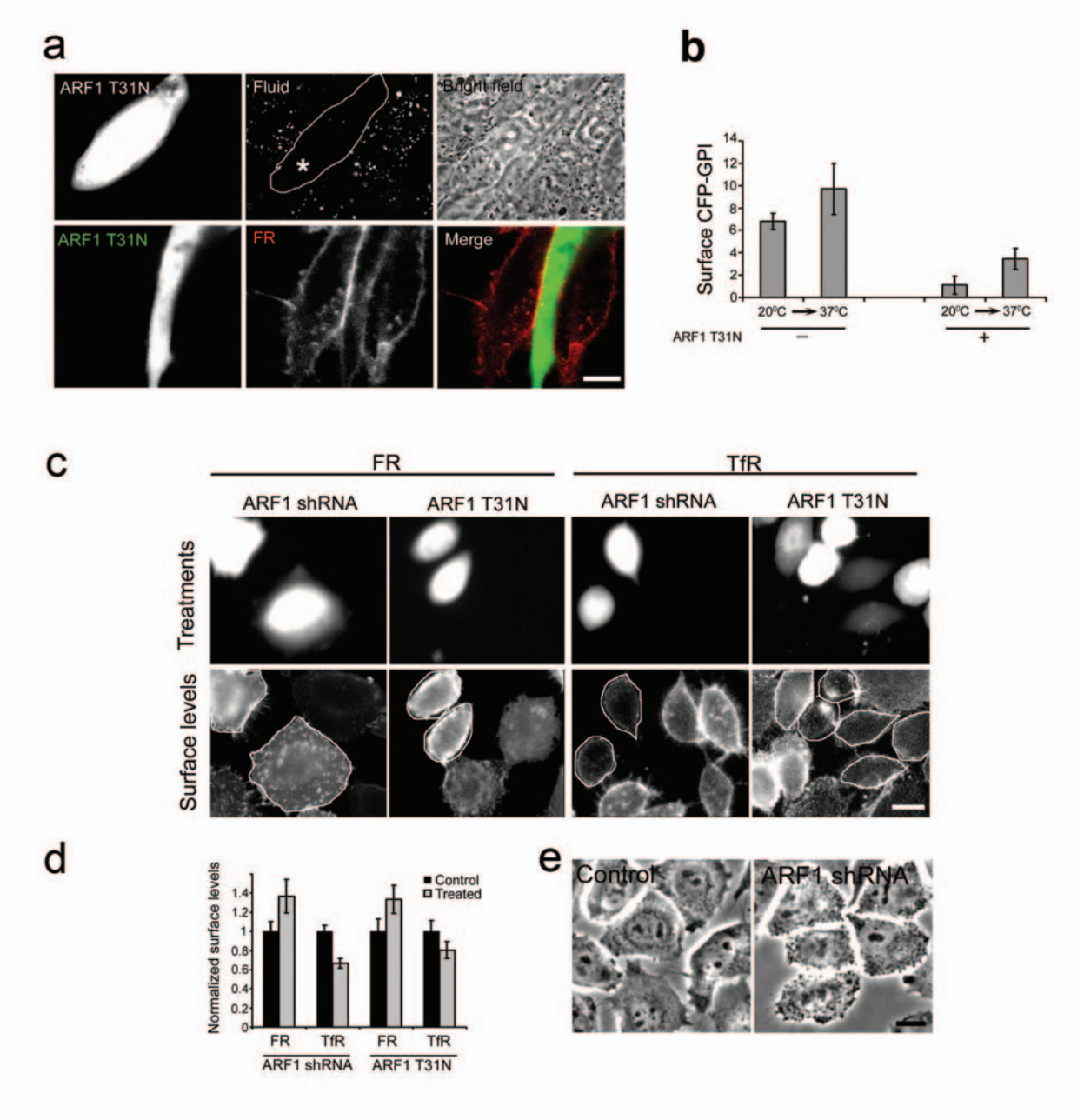

Figure S2 Dominant-negative ARF1 expression inhibits endocytosis via GEEC in multiple cell types, and also blocks exocytosis of GPI-APs. (a) *ARF1-T31N expression inhibits fluid-phase and GPI-AP endocytosis in different cell type.* BHKs transfected with ARF1-T31N for 20h, were pulsed with TMR-Dex or Alexa^{647}Mov19 for 5min and processed for imaging. Single confocal planes from a stack of images show the extent of internalized cargo. Note fluid-phase uptake (upper panel) and FR-GPI uptake (in cells with comparable surface FR-GPI expression), are inhibited in transfected cells (*). ≥ 60% of ARF1-T31N transfected cells show obvious downregulation of fluid-phase and FR-GPI uptake. (**b**) *GPI-AP exocytosis is inhibited by ARF1-T31N expression.* IA2.2 cells were transiently transfected with CFP-GPI, either alone (-) or with ARF1-T31N (+), for 12h and shifted to 20°C, and incubated for additional 8h in HEPES-buffered growth medium. Surface levels of CFP-GPI were monitored before (20°C) and after chase for 1h at 37°C in presence of cycloheximide (37°C). Histogram shows quantification of anti-CFP fluorescence detected at the cell surface normalized to total CFP expression per cell. Bars represent weighted mean from two independent experiments +/- SEM. n≥35. This experiment was repeated twice with similar results. While the level of total CFP-GPI was similar, ARF1-T31N reduces net CFP-GPI secretion (compare surface levels of CFP-GPI before and after 1h 37°C chase, with and without ARF1-T31N expression, respectively). **c-e)** *Modulation of ARF1 levels and activity affect steady state cell surface levels of TfR and FR-GPI.* IA2.2 cells transfected with ARF1-T31N for 16h or ARF1 shRNA for 62h, were incubated with saturating amounts of Cy5-labelled Okt9 or Cy5-labelled Mov19 at 4°C for 1h, fixed and imaged. Cells expressing the indicated constructs (upper panels) exhibit altered receptor levels (lower panels, transfected cells outlined). **(d)** Histogram shows surface levels of receptors in transfected and control cells, normalized to control. Bars represent weighted mean from two independent experiments +/- SEM. n≥75. **(e)** Cells transfected with ARF1 shRNA to deplete ARF1 levels show more spikes-like, filopodial structures compared to cells transfected with a control vector.

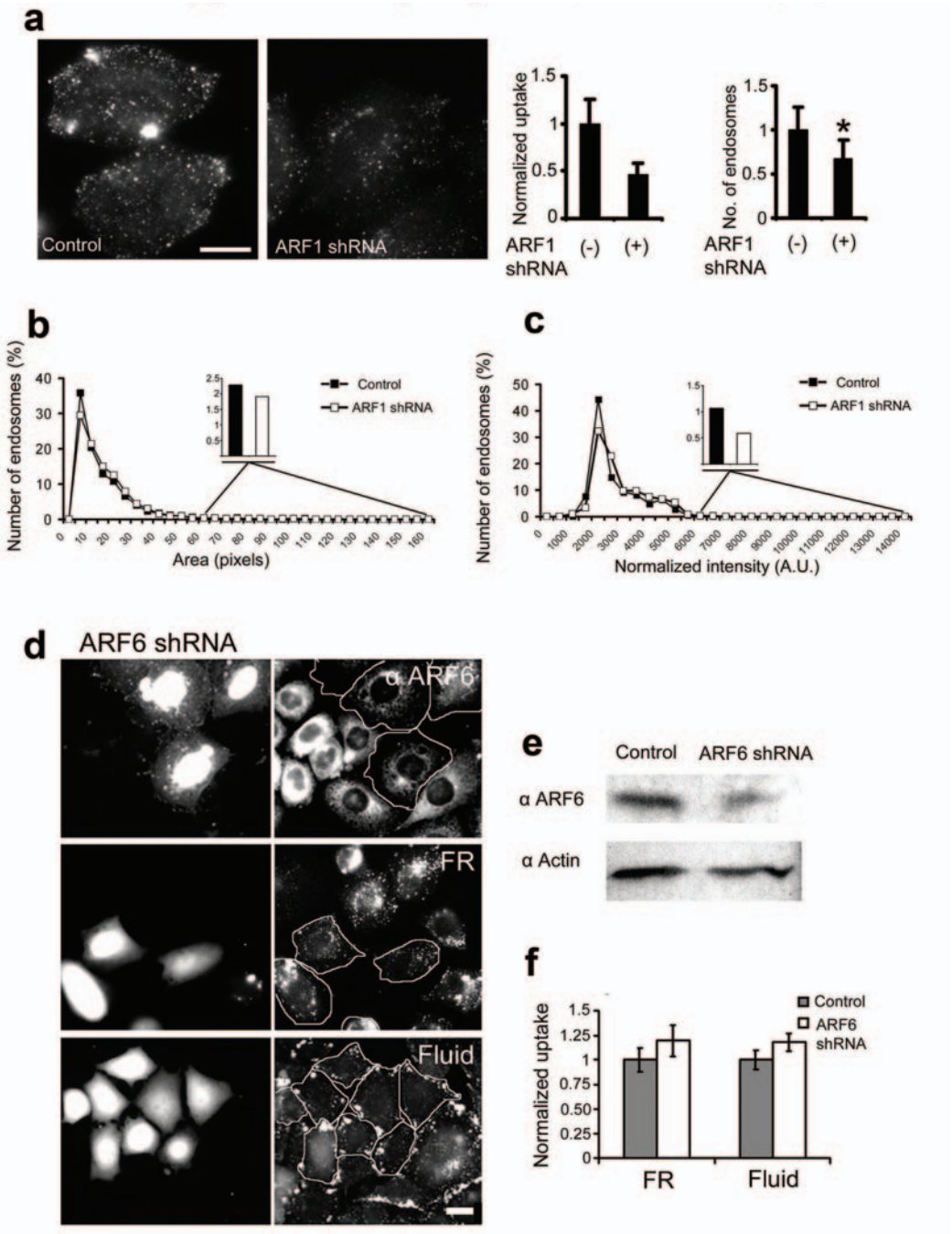

Figure S3. Depletion of ARF1 affects number and amount of endocytosed probe in GEECs whereas depletion of ARF6 is without any effect. **(a-c)** *Effect of ARF1-depletion on endosomal parameters:* Control and ARF1 shRNA-transfected IA2.2 cells were pulsed with TMR-Dex for 3min at 37°C, fixed and imaged at high magnification and resolution (**a**; 60X, 1.4NA). Endosomes were identified and counted (Methods). Histograms show the average integrated fluid uptake per cell normalized to that measured in control cells (Left histogram, *p*value, 0.003) and average number of fluid endosomes per cell (right histogram). Each bar represents average value +/- SD, n≥15. Graph shows the distribution of endosomes with respect to area (**b**; no. of pixels) and fluorescence intensities of endosomes **(c)** identified as above in control and ARF1-depleted cells. The number of endosomes is normalized to the total number of endosomes in each condition. Insets represent total fraction of endosomes present in the indicated bins. Note in ARF1-depleted cells while the net number and total uptake is lower (histogram in **a**), the shape of the endosomal population in terms of range of sizes (**b**; area) is almost identical to the control cells. There is a small difference in the fraction of very low (peak endosomal values in **c**) and very high intensity endosomes (inset in **c**). **(d-f)** *Effect of ARF6-depletion:* To examine the role of ARF6 in endocytosis via GEECs, IA2.2 cells were transfected with ARF6 shRNA in pGSUPER vector for 60h and processed for immunofluorescence (**d**, Top panel) or western blot **(e)** for assessing the extent of reduction of ARF6 protein, or assessed for their ability to endocytose FR-GPI (a, middle panel) or the fluid phase (a, bottom panel) by pulsing with PLR or TMR-Dex, respectively for 10min. Left panels in **(d)** show GFP-expression in cells transfected with ARF6 shRNA; corresponding cells are outlined in right panels in **(d)**. Histogram **(f)** shows the quantification of uptake of fluid-phase and FR-GPI in control and ARF6-depleted cells where endocytosed probe fluorescence is normalized to that measured in control cells. PLR-uptake is normalized to FR-GPI surface levels in each cell. Bars represent weighted mean from two independent experiments +/- SEM. n≥85.

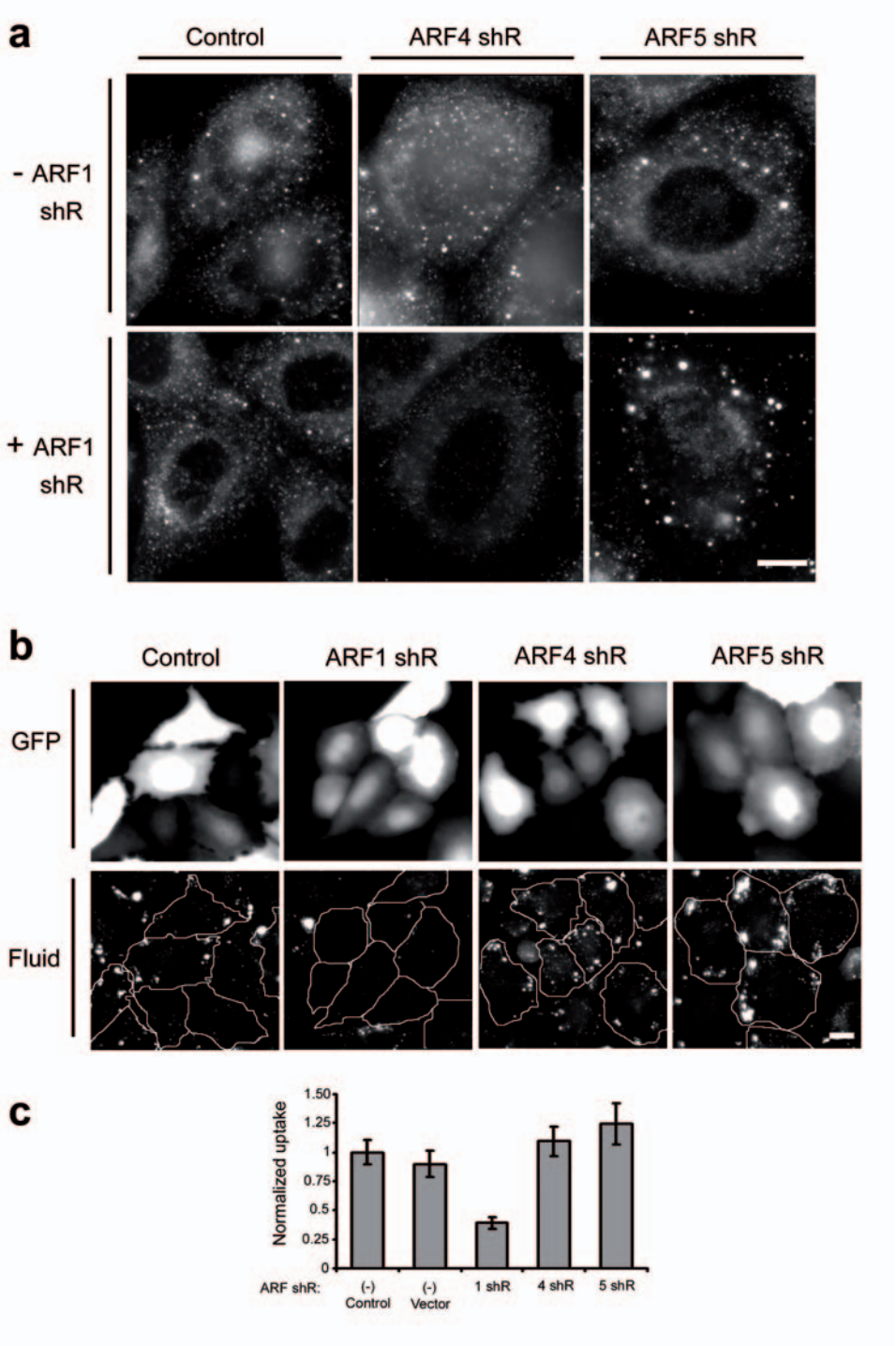

Figure S4. Uptake into GEECs is insensitive to depletion of ARF4 and ARF5. **(a)** IA2.2 cells were transfected with either ARF4 shRNA or ARF5shRNA (upper panels) or along with ARF1 shRNA (lower panels) were stained for βCOP. Transfected cells were identified with GFP expression (corresponding images not shown). Note that while cell expressing ARF1 and ARF4 shRNAs (lower middle panel) has dispersed staining of βCOP, cells expressing ARF1 and ARF5 shRNAs have large cytoplasmic βCOP-containing inclusion like structures. This phenotype is seen in ≥70% of transfected cells, n≥25. **(b)** IA2.2 cells were co transfected with eGFP-N1 with vector (control) or ARF1 or ARF4 or ARF5 shRNAs and were pulsed with TMR-Dex for 5min, washed, fixed and imaged. The images show fluid uptake (lower panels) in cells transfected with shRNAs (upper panels). Histogram in **(c)** shows quantitation of fluid uptake in indicated expression backgrounds. Each bar represents weighted mean of average intensities from two independent experiments, normalized to the control, +/- SEM.

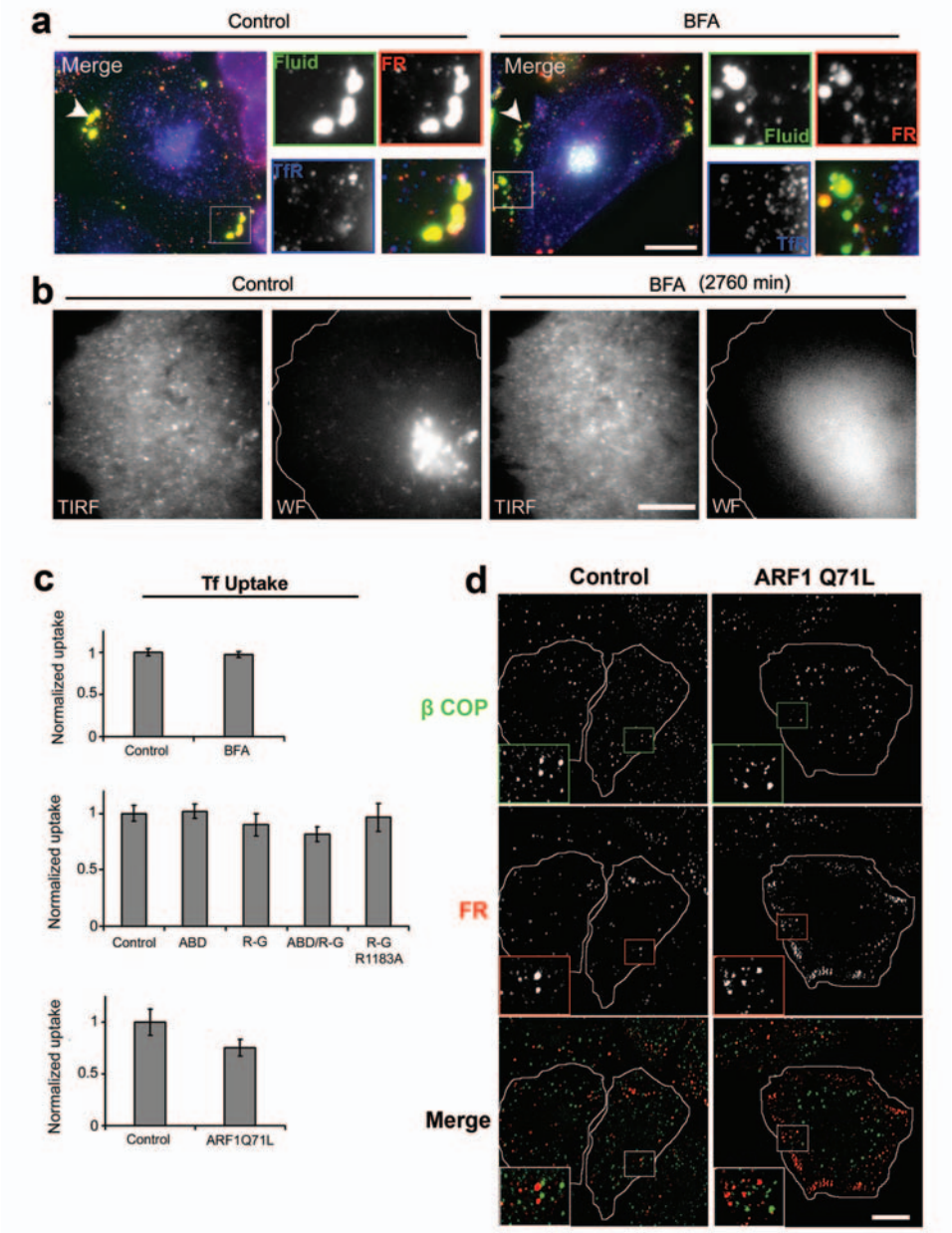

Figure S5. Effects of Brefeldin A and ARHGAP10 or ARF1-Q71L expression on endocytosis, ARF1-localization, and COPI localization. **(a-b)** *Brefeldin A-treatment enhances endocytosis via the GEEC pathway, and does not affect plasma membrane ARF1 localization.* IA2.2 cells were treated with 20μg/ml BFA for 60min and pulsed with PLF, TMR-Dex and Alexa^{647}-Tf during the last 10min **(a)**. After termination of pulse with washing, cells were processed for live imaging (Methods). Arrowheads in merge of fluid (green), FR-GPI (red) and TfR (blue) show endosomes of GEEC pathway, which are devoid of endocytosed TfR in control and treated cells. Note while the number and extent of endocytosis in BFA-treated cells in enhanced (quantification in Fig.4b), the endosomes still remain separate from endocytosed TfR, consistent with their identity as GEECs. Separately, IA2.2 cell transfected with ARF1-GFP was imaged live under TIRF and widefield (WF) illumination sequentially with a lag of 200msec **(b)**. The images are snapshots from a time course of BFA treatment on microscope stage. Note that after BFA treatment, while distribution on Golgi is altered drastically (WF), at PM, the punctate structures that mark sites of activated ARF1 remain unaltered. The overall levels of ARF1 in TIRF normalized to widefield increases marginally (data not shown). **(c)** *Effects of BFA treatment, overexpression of ARHGAP10 mutants and ARF1-Q71L on TfR uptake.* IA2.2 cells were pulsed with Alexa^{568}-Tf for the 10min. Surface Tf was removed and cell surface TfR levels were measured using ice labeling with Cy5-Okt9. The **top histogram** shows the ratio of Tf uptake in treated (BFA; 20μg/ml, 1h) and untreated (control) cells normalized to surface receptor expression in each cell, and plotted as a ratio of the uptake in control cells. Data are weighted mean from two independent experiments +/- SEM. n≥150. In the **middle histogram,** IA2.2 cells transfected with cDNAs expressing indicated constructs for 16h were pulsed with Tf and uptake was quantified as above; the ratio of Tf uptake and surface receptor expression per cell in transfected cells was normalized to that measured in control cells. Data are weighted mean from two independent experiments +/- SEM. n≥35. In the **bottom histogram,** IA2.2 cells transfected with pEGFP-N1 alone or with ARF1-Q71L for 16h were pulsed with Tf as above and the extent of Tf-uptake quantified. Data in histogram is weighted mean of average from two experiments, +/-SEM. n≥70. All of the above-mentioned experiments were repeated twice with similar results. **(d)** *ARF1-generated GEECs do not co-localize with COPI.* CHO cells transfected with GFP alone (Control) or with HA-ARF1-Q71L were pulsed with Cy3-MoV19 Fabs for 5min, surface fluorescence was removed and cells were processed for immunofluorescence and imaged on a confocal microscope. Single confocal plane from a stack of images are shown where peripheral endosomes formed in presence or absence of ARF1-Q71L are clearly visualized. These structures do not co-localize with β-COP staining which is prominently visualized on the perinuclear vesicular structures in other confocal planes (data not shown).

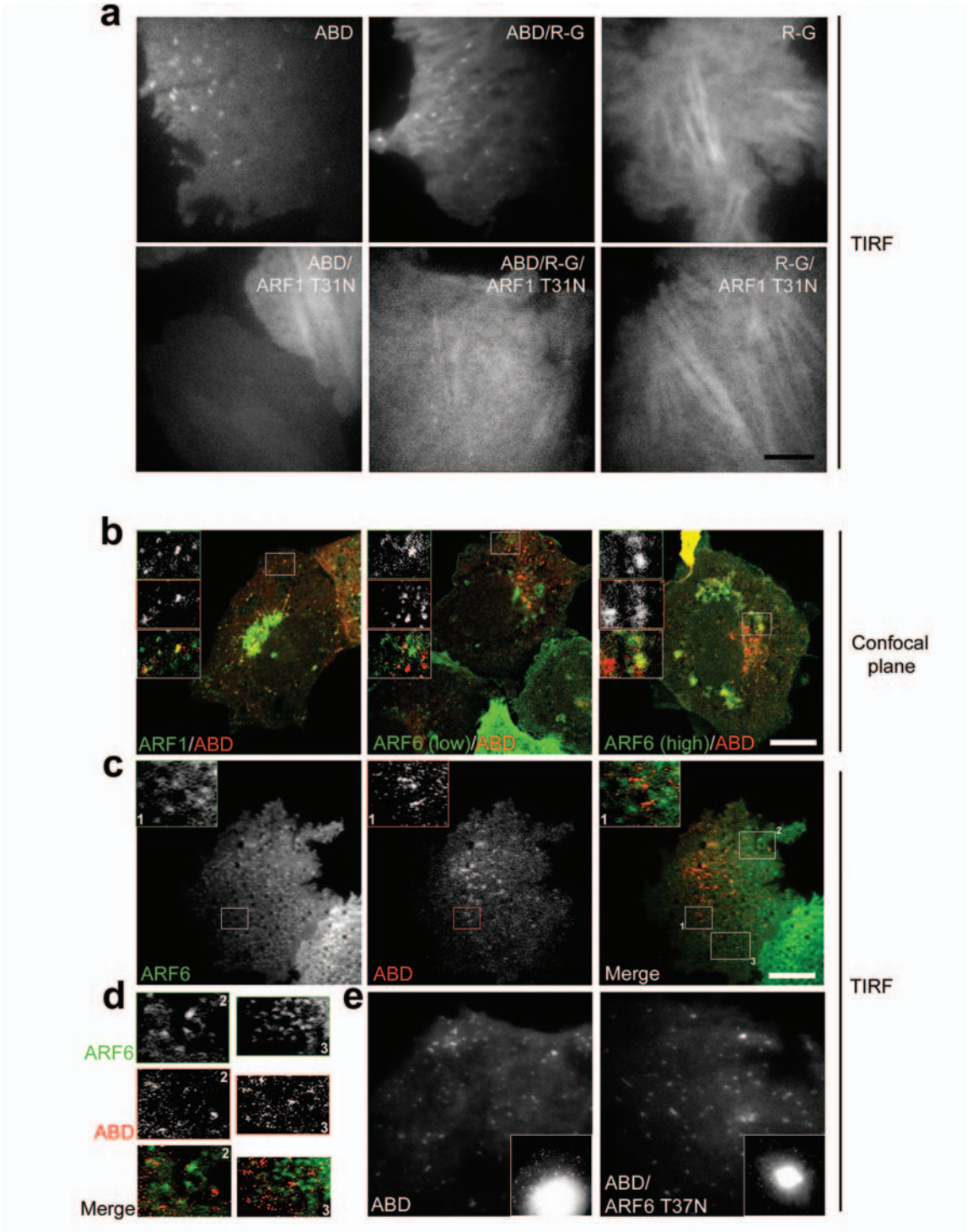

Figure S6. ABD domain of ARHGAP10 and activation of ARF1 is required for the localization of ARHGAP10 at the PM. (**a**) IA2.2 cells transfected with GFP-ABD, GFP-ABD/R-G, or GFP-R-G domains of ARHGAP10 (see Fig.5a) alone (top panels) or along with ARF1-T31N (bottom panels) were imaged in TIRF field. Note only ABD-containing domains are recruited to the cell surface in a punctate distribution. This recruitment is sensitive to ARF1 activity since it is inhibited by co-expression of ARF1-T31N. (**b**) IA2.2 cells co-transfected with RFP-ABD along with ARF1-GFP (left panel) or ARF6-GFP (middle and right panels) were imaged using confocal microscopy. Each image represents merge of single confocal plane showing ARF1 (green) and ABD (red) distribution. Insets are magnified regions demarcated with square in corresponding source image. Note that while most ABD structures colocalize with ARF1, the colocalization with ARF6 is seen only at high expression levels of ARF6 (right panel), a scenario where still fraction of ABD is independent of ARF6, marking a perinuclear Golgi-like structure. n≥20. This experiment was repeated twice with similar results. (c-f) IA2.2 cells cotransfeced with ARF6-GFP and RFP-ABD were imaged live under TIRF illumination. Note that the overall distribution of ABD is distinct from ARF6. Insets in (c) and the panels in (e) are magnified from the regions marked with square in "merge" panel in (**c**). (**f**) The distribution of ABD at or near PM is not sensitive to ARF6 activity. Cells transfected with ABD alone (left panel) or cotransfected with HA-ARF6-T37N were imaged using TIRF and wide-field illumination. The distribution of ABD at the PM is unaltered upon co-expression of ARF6-T37N. Insets show corresponding whole-cell widefield images. n≥25.

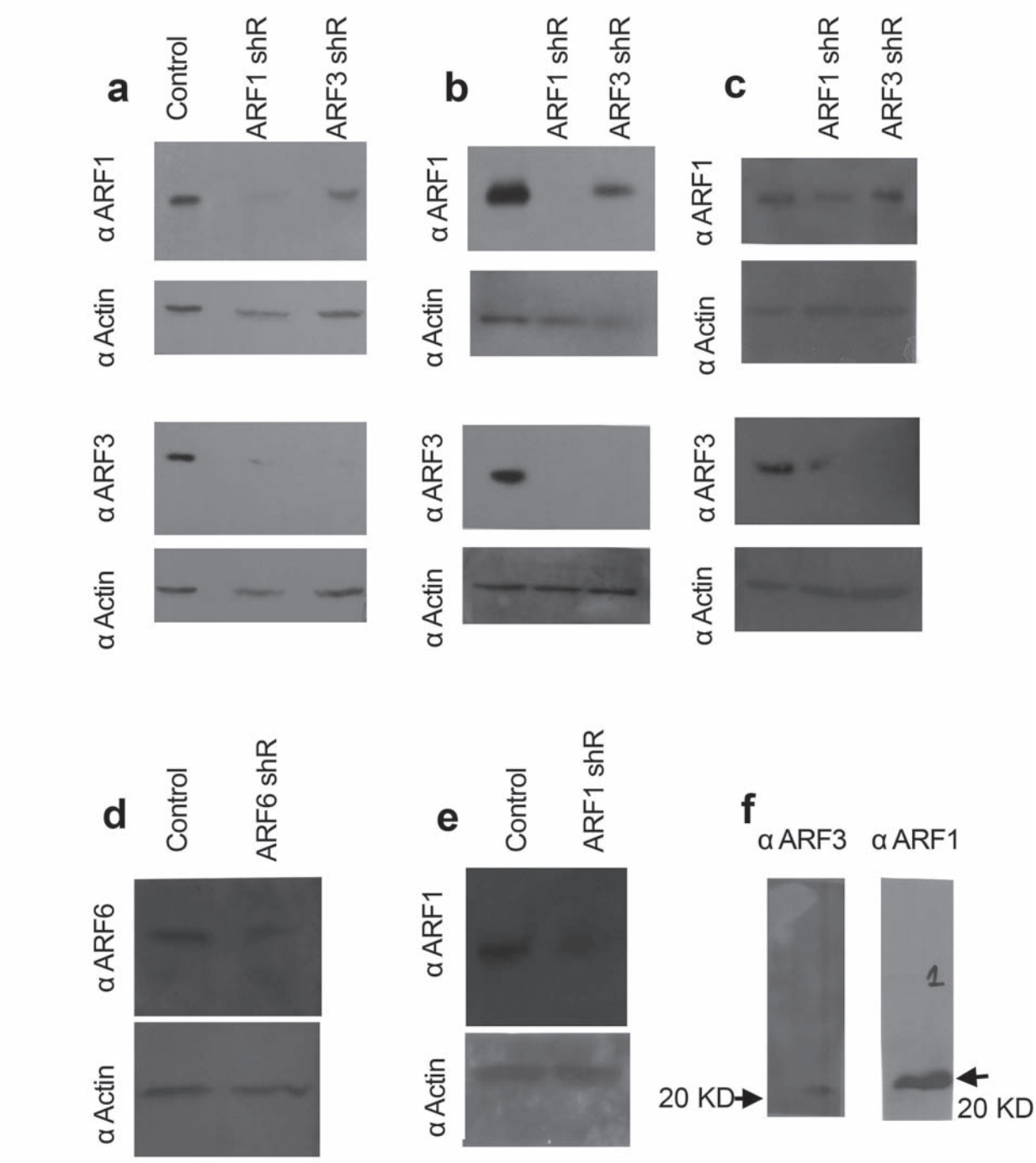

Figure S7 Western blots used in the study. (**a**), (**b**), (**c**) represent the blots obtained from three independent experiments respectively, used in quantitation of ARF1 and ARF3 depletion in Fig.2b. Western blotting was carried out as described in methods. In all blots, first lane represents vector transfected cells (control), second lane and third lane represent lysates from cells transfected with ARF1 shRNA and ARF3 shRNA respectively. Corresponding actin levels (from the respective lysates in the same membrane) are shown immediately below the ARF lanes. Blot in (d) shows membrane probed for ARF6 in control and ARF6 shRNA transfected cells and is original of the blot used in supplementary fig. S3e. (**e**) represents the original of the blot used in Fig.2e. Blots shown in (**f**) are antibody-specificity controls, for ARF3 and ARF1 antibodies respectively. Both antibodies were found to detect single bands when used to probe control cell lysate using mentioned procedure (Methods). ARF1 antibody (Affinity Bioreagents, detects ARFs, MA3-060, generated for recombinant human ARF1) also detects overexpression of ARF1-GFP (Fig.3c) in an expression-dependent manner in immunofluorescence in CHO cells (data not shown) and is sensitive to reduction in ARF1 levels by shRNA. Anti-ARF3 antibody [4,5] (BD transduction laboratories, catalogue no.610785, generated for human ARF3) similarly detects single band in control cell lysates. Polyclonal anti-ARF6 antibody was kind gift of Dr. Sylvain Bourgoin (University of Alberta, Canada). All primary antibodies were used at a dilution of 1:100 and rabbit Anti-actin (Sigma Chemicals, A5060) was used at 1:1000 in 1% blotto in TTBS solution. HRP-conjugated secondary antibodies (Jackson Immunoresearch) were used at a dilution of 1:5000). All the blots are presented in original, non-processed forms. For quantitation from (a,b,c), The scanned images were inverted using Adobe Photoshop™ , background subtracted and quantitated using Metamorph™ software. After obtaining per band intensity, the quantitations were carried out as described in Fig.2b legends.

SUPPLEMENTARY MOVIE LEGENDS

Movie 1 Dynamics of ARF1-GFP (right) and GFP-ABD (left) on PM. CHO cells expressing very low levels of GFP-tagged proteins were imaged using TIRF microscopy, with 100msec exposure time and stream acquisition (10 frames/sec). Playback rate is 1.6 times faster than acquisition rate. Scale bar represents 10μm.

Movie 2 Dynamics of Cdc42 in the TIRF field in cells transfected with control vector (left) or with shRNA for ARF1. CHO cells expressing low levels of Cdc42-GFP were imaged using TIRF microscopy, with 100msec exposure time and stream acquisition (10frames /sec). Playback rate is same as the acquisition rate. Scale bar represents 10μm.

Supplementary Text for Kumari and Mayor

Supplementary Materials and Methods

Materials:

Chemicals, inhibitors and reagents were purchased from Sigma Chemicals Co. (St. Louis, MO), unless otherwise specified. TMR-Dex and amine-reactive fluorophores were purchased form Molecular probes (Eugene, OR). Fluorophores were tagged to different proteins according to manufacturer's instructions, and optimal dye to protein ratios obtained. Fluorescent folate analogs N^{α}-pteroyl-N^{ε}-(4'-fluorescein-thiocarbamoyl)-L-lysine (PLF) or N^{α}-pteroyl-N^{ε}-(4'- lissamine rhodamine-thiocarbamoyl)-L-lysine (PLR) were synthesized by Dr. Ram Vishwakarma (NII, New Delhi) and was used at 40nM and 200nM, respectively, as described previously [1]. *N*- (4, 4-difluoro-5, 7-dimethyl-4-bora-3a, 4a-diaza-*s*-indacene-3-pentanoyl (BODIPY)-lactosylceramide (C_6-LacCer) was kind gift from Dr. Richard E. Pagano (Mayo Clinic and Foundation, Rochester). HRP and TMB were purchased from Bangalore Genei (Bangalore, India).

Cells and transfection:

CHO cells or CHO cells stably expressing FR-GPI and human TfR (IA2.2 cells) were used for most of endocytic assays, as before [2]. CHO cells were grown in HF-12 (HiMEDIA, Mumbai, India; CHO) while others (MEF, BHK) in DMEM, both containing $NaHCO_3$, 100μg/ml penicillin, streptomycin and supplemented with 10% FBS (GibcoBRL, Rockville, MD). Cells were transfected with different DNA constructs using FuGENE6 (Roche Diagnostics, GmbH Deutschland) according to manufacturer's protocol. For transfections in MEFs, Effectene (Quiagen) was used. In cotransfection studies, DNA ratios were optimized to obtain coexpression of expressed proteins, and independently confirmed by

immunofluorescence. Endocytic assays were carried 18-20 hours following transfection, unless otherwise indicated. Cell health was assessed using Trypan-blue exclusion and in all cases, transfected cells were indistinguishable from untransfected cells or control cells; >98% of cells excluded Trypan-blue regardless of the transfection employed (data not shown). In the images shown in supplementary figures, Scale bar represents 10μm, unless otherwise specified.

Antibodies:

Anti-HA mouse monoclonal antibody (6E2) and anti-V5 antibodies [Cell Signaling Technology (Beverly, MA)], anti-actin antibody (Sigma Chemical Co.), anti-ARF3 monoclonal antibody [BD Transduction laboratories (San Diego, CA)] were used for western blotting and immunofluorescence as indicated. Anti-ARF6 rabbit polyclonal serum was a kind gift of Dr. Sylvain Bourgoin (University of Alberta, Canada); anti-ARF1 antibody was a generous gift of Affinity Bioreagents (Golden, Co, USA). Fab fragments of anti-GFP and anti-FR MoV19 monoclonal antibodies generated using papain digestion subsequently fluorescently labeled and were used for monovalent receptor binding for endocytosis assays as described [2]. Anti-TfR monoclonal antibody was purified from mouse hybridoma, OKT9 (National Centre for Cell Science, Pune, India). Anti- IL2-β monoclonal antibody (561) was kind gift of Dr. A. Dautry-Varsat (Institut Pateur, France).

Plasmids:

ARF1-GFP WT and dominant negative (T31N mutant) constructs were obtained from Dr. J. Gruenberg (University of Geneva). HA–tagged ARF1-WT, Q71L and T31N expressing constructs were obtained from Dr. Ferguson (Robarts Cell Biology Research Institute, Ontario, Canada). GFP-ARHGAP10 and related constructs, and ARF1, ARF3, ARF4 and ARF5 specific shRNA were provided by were kindly provided by Dr. Philip

Chavrier (Institut Curie, France), and Dr. Richard A. Kahn (Emory University), respectively. V5-tagged N-terminal fragment of ARHGAP10 used for assessing shRNA-mediated depletion were obtained from Dr. Pascale Cossart (Institut Pasteur, France). IL2-β expression plasmid was was kind gift of Dr. A. Dautry-Varsat (Institut Pateur, France). GFP and HA-tagged ARF6 constructs were provided by Dr. J. Donaldson (National Institutes of Health, USA).

Table 1

	ShRNA target	Sequence (5'-3')
1.	ARF1 [3]	ACCGTGGAGTACAAGAACA
2.	ARF1[3]	TGACAGAGAGCGTGTGAAC
3.	ARF3 [3]	ACAGGATCTGCCTAATGCT
4.	ARF4 [3]	TCTGGTAGATGAATTGAGA
5.	ARF5 [3]	TCTGCTGATGAACTCCAGA
6.	ARF6 (this study)	CCAGGAGCTGCACCGCATTAT
7.	ARHGAP10 (this study)	GTCATTGTGCCTTCTGAGA

Endocytic and exocytic assays and immunofluorescence:

Endocytic and exocytic assays cells were carried out as described [2] with minor modifications. Briefly, endocytosis of FR-GPI or TfR was monitored by labeling cells with fluorescently tagged Mov19 Fabs (5μg/ml) or Tf (10μg/ml) incubated at 37°C for indicated times. The pulse was terminated by cooling cells on ice and washing with chilled HEPES-buffered isotonic buffer (M1:140mM NaCl, 20mM HEPES, 1mM $CaCl_2$, 1mM $MgCl_2$, 5mM KCl, pH 7.4). To remove surface fluorescence, cells were treated with PI-PLC (50μg/ml, 1h; GPI-APs) or with ascorbate buffer (160mM sodium ascorbate, 40mM ascorbic acid, 1mM $MgCl_2$, 1mM $CaCl_2$, pH 4.5; Tf) at 4°C and subsequently fixed with 2% paraformaldehyde for 15min. Similarly, for fluid-phase and CTx uptake, cells were incubated with 1mg/ml fluorescently-labeled dextran or 1μg/ml CTx at 37°C. C_6-LacCer endocytosis was monitored by surface labeling cells with C_6-LacCer. C_6-LacCer was (2.6mM in ethanol) dissolved in 0.15% defatted BSA to achieve a concentration of 100μM. The BSA-lipid complexes was dialyzed against PBS at 37ºC for 20min to remove ethanol and used for endocytosis assays. IA2.2 cells pre-incubated in serum-free medium for 1h, and prior to incubation with 200nM BSA-lipid complexes on ice for 20min. Subsequent to washing, cells were chased at 37°C for 5min in presence of $Alexa^{647}$-Dex (2mg/ml). The pulse was terminated by washing with chilled M1 on ice and surface C_6-LacCer was back-extracted by incubation of cells with 5% solution of defatted BSA in M1 at 4°C for 30min. Cells were subsequently fixed and imaged. In some experiments, cells were processed for immunostaining post-fixation. For HRP uptake, cells were plated in 92mm dishes, transfected with vector alone or ARF1 shRNA for 72h. Cells were pulsed with 1mg/ml HRP for 10min at 37ºC, then washed with chilled M1 and ascorbate buffer and

subsequently incubated with 5mg/ml BSA on ice. Cells were then scraped off the dish, counted and lysed using RIPA buffer (150mM NaCl, 50mM Tris-HCl, pH 7.5, 500μM EDTA, 100μM EGTA, 1.0% Triton X-100, and 1% sodium deoxycholate). Cell lysates from equal numbers of cells were used for total protein estimation and HRP activity. HRP activity was measured by monitoring the absorbance of reaction product, upon the incubating with equal amounts of H_2O_2/TMB solution, at 450nm on ELISA reader (BioRad).

To quantify CFP-GPI exocytosis, cells were plated in HEPES-buffered HF-12, transfected with CFP-GPI DNA and post-transfection (10h), transferred to restrictive temperature of 20°C. After 12h at 20°C, cells were incubated with 50μg/ml cycloheximide for an additional hour, followed with 1h at 37°C along with cycloheximide, with or without BFA, washed with pre-chilled M1, incubated with fluorescently labeled anti-GFP monoclonal antibody, and fixed prior to imaging.

In the immunofluorescence assays, cells were fixed and permeabilized with 0.5% Tween20 for 20min and then incubated with primary and fluorescently labeled secondary antibody where necessary. Under these conditions, minimal loss of fluid-phase endocytic tracers was detected.

References:

1. Sharma, P. *et al.* Nanoscale organization of multiple GPI-anchored proteins in living cell membranes. *Cell* **116**, 577-589 (2004).
2. Sabharanjak, S., Sharma, P., Parton, R.G. & Mayor, S. GPI-anchored proteins are delivered to recycling endosomes via a distinct cdc42-regulated, clathrin-independent pinocytic pathway. *Dev Cell* **2**, 411-423 (2002).

3. Volpicelli-Daley, L.A., Li, Y., Zhang, C.J. & Kahn, R.A. Isoform-selective effects of the depletion of ADP-ribosylation factors 1-5 on membrane traffic. *Mol Biol Cell* **16**, 4495-4508 (2005).
4. Dusanka Deretic, Valerie Traverso, Nilda Parkins, Fannie Jackson, Elena B. Rodriguez de Turco, and Nancy Ransom. Phosphoinositides, Ezrin/Moesin, and Rac1 regulate fusion of Rhodopsin Transport Carriers in retinal photoreceptors. *Mol Biol Cell* **15**, 359–370, (2004).
5. Aminul Islam, Xiaoyan Shen, Toyoko Hiroi, Joel Moss, Martha Vaughan, and Stewart J. Levine. The Brefeldin A-inhibited Guanine Nucleotide-exchange protein, BIG2, regulates the constitutive release of TNFR1 exosome-like vesicles. *J. Biol Chem*. **282(13)**, 9591–9599, (2007).